AGU ADVANCING EARTH AND SPACE SCIENCE

Paleoceanography and Paleoclimatology

RESEARCH ARTICLE
10.1029/2020PA003949

Key Points:

- We present an SW Pacific Ocean lithogenic flux record for the last 410 ka that covaries with the Antarctic and sub-Antarctic dust records
- Westerly wind-transported material from New Zealand is the most likely dust source over glacial-interglacial cycles
- Silt-sized sediment was well sorted by bottom currents, which were more energetic in interglacials than glacials

Supporting Information:

Supporting Information may be found in the online version of this article.

Correspondence to:

Y. Wu,
wuy@scsio.ac.cn

Citation:

Wu, Y., Roberts, A. P., Grant, K. M., Heslop, D., Pillans, B. J., Zhao, X., et al. (2021). Climatically modulated dust inputs from New Zealand to the Southwest Pacific sector of the Southern Ocean over the last 410 kyr. *Paleoceanography and Paleoclimatology*, *36*, e2020PA003949. https://doi.org/10.1029/2020PA003949

Received 10 APR 2020
Accepted 2 MAR 2021

Climatically Modulated Dust Inputs from New Zealand to the Southwest Pacific Sector of the Southern Ocean Over the Last 410 kyr

Yi Wu[1,2,3], Andrew P. Roberts[2], Katharine M. Grant[2], David Heslop[2], Brad J. Pillans[2], Xiang Zhao[2], Eelco J. Rohling[2], Thomas A. Ronge[4], Mingming Ma[5], Paul P. Hesse[6], and Alan S. Palmer[7]

[1]Key Laboratory of Ocean and Marginal Sea Geology, South China Sea Institute of Oceanology, Innovation Academy of South China Sea Ecology and Environmental Engineering, Chinese Academy of Sciences, Guangzhou, China, [2]Research School of Earth Sciences, Australian National University, Canberra, ACT, Australia, [3]Southern Marine Science and Engineering Guangdong Laboratory (Guangzhou), Guangzhou, China, [4]Alfred Wegener Institut Helmholtz-Zentrum für Polar- und Meeresforschung, Bremerhaven, Germany, [5]School of Geographical Sciences, Fujian Normal University, Fuzhou, China, [6]Department of Earth and Environmental Sciences, Macquarie University, Sydney, ACT, Australia, [7]School of Agriculture and Environment, Massey University, Palmerston North, New Zealand

Abstract Eolian mineral dust is an active agent in the global climate system. It affects planetary albedo and can influence marine biological productivity and ocean-atmosphere carbon dynamics. This makes the understanding of the global dust cycle crucial for constraining the dust/climate relationship, which requires long-term dust emission records for all major dust sources. Despite their importance, the sources of atmospheric dust deposited in the Southern Ocean remain poorly constrained. Eolian dust in the Pacific sector of the Southern Ocean is generally assumed to originate from Australia, with minor contributions from New Zealand. Here, we present a high-resolution elemental record of terrestrial inputs for the past ~410 kyr from marine sediment core PS75/100-4 recovered from east of South Island, New Zealand. Sediment grain size is slightly finer than that of loess deposits from South Island, New Zealand, and is coarser than that of marine sediments in the Tasman Sea to the west of New Zealand, which indicates that the dust originated mainly from New Zealand and not only from Australia. Core PS75/100-4 records lithogenic mass accumulation rates ranging from ~0.01 to 0.69 g/cm^2/kyr (~0.20 g/cm^2/kyr average), with variations over a factor of ~3–4 over glacial versus interglacial timescales for the past 410 kyr. Our geochemical data correlate well with the Southern Ocean and Antarctic eolian dust records and suggest a westerly wind-supplied dust signal from New Zealand. Our findings, therefore, suggest that New Zealand should be considered an important long-term regional dust source in global dust cycle models.

1. Introduction

The global mineral dust cycle is a key part of the climate system (An et al., 1991; Guo et al., 2002; Hovan et al., 1989; Lambert et al., 2008; Lamy et al., 2014; Liu, 1985; Maher et al., 2010; Mahowald et al., 2006; Martínez-García et al., 2011; Prospero et al., 2002; Rea, 1994; Rea et al, 1985, 1998; Shao et al., 2011). Dust changes the radiative properties of the atmosphere by scattering and absorbing solar and terrestrial radiation, and influences climate both directly and through cloud-nucleation processes (Köhler et al., 2010; Lohmann & Feichter, 2005; Maher et al., 2010; Masson-Delmotte et al., 2010; Rohling et al., 2012). Dust deposition onto the ocean surface may also affect climate indirectly by supplying iron as a micronutrient to Fe-limited waters, thereby fertilizing phytoplankton productivity, which results in atmospheric CO_2 drawdown (Jickells et al., 2005; Kohfeld & Harrison, 2001; Martin et al., 1991; Martínez-García et al., 2014; Moore et al., 2013; Shoenfelt et al., 2018, 2019; Tagliabue et al., 2017).

Global dust fluxes were generally greater (~2–5 times) during glacials than during interglacials throughout most regions and varied spatially (e.g., Kohfeld & Harrison, 2001; Maher et al., 2010 and references therein). This makes it important to obtain atmospheric dust records for all of the world's major dust source regions over glacial-interglacial (G-IG) timescales to understand the role of the dust cycle in long-term climate forcing. Mid-latitude arid regions, such as the Sahara and Sahel, the Middle East, and the Asian interior in the Northern Hemisphere, and the Namib Desert, Patagonia, and Australian deserts in the Southern

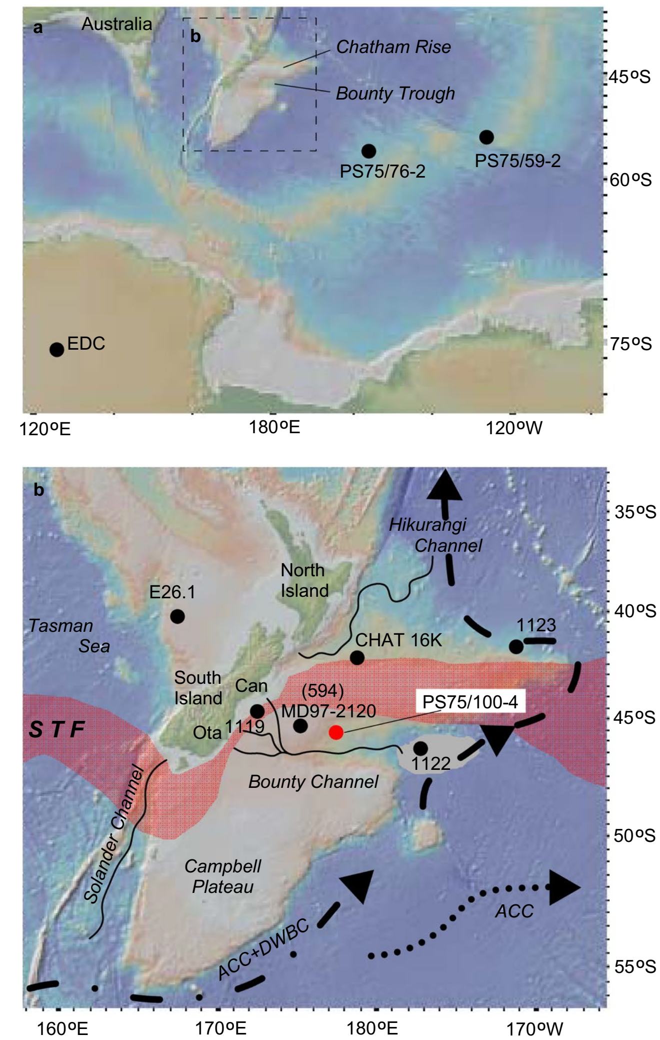

Figure 1. Location maps for studied sediment core PS75/100-4 (red circle). (a) Black circles mark core sites discussed in the text: Southern Ocean Pacific Sector cores PS75/76-2 (55°31.71′S, 156°8.39′W; 3,742 m water depth) and PS75/59-2 (54°12.90S, 125°25.53′W; 3,613 m water depth); Antarctic EDC ice core (76°6′S, 123°21′E); (b) Deep Sea Drilling Project (DSDP) Site 594 (45°31.41′S, 174°56.88′E; 1,204 m water depth); core MD97-2120 (45°32.06′S, 174°55.85′E; 1,210 m water depth), as a reoccupation of DSDP Site 594; Ocean Drilling Program (ODP) Site 1119 (44°45.332′S, 172°23.598′E; 396 m water depth); ODP Site 1122 (46°34.781′S, 177°23.610′W; 4,432 m water depth), located on Bounty Fan (indicated by the gray zone); ODP Site 1123 (41°47.2′S, 171°29.9′W; 3,290 m water depth); core CHAT 16K (42°32.00′S, 178°29.92′E; 1,408 m water depth); and Tasman Sea core E26.1 (28 cm in length; 40°17′S, 168°20′E; 910 m water depth). Black lines in (b) indicate locations of the main submarine channels (Solander, Bounty, and Hikurangi Channels) through which sediment is transported around New Zealand. "Can" and "Ota" indicate the Canterbury and Otago regions of South Island, New Zealand, respectively. The paths of the deep western boundary current (DWBC, black dashed lines) and the Antarctic Circumpolar Current (ACC), which flow east of New Zealand, are modified from Hall et al. (2001). The red belt in (b) represents flow along the Subtropical Front (STF). Dust can be carried to the studied core site by westerly winds from potential source areas in New Zealand and Australia. The maps were produced using www.geomapapp.org.

Hemisphere, are major eolian dust source areas. Based on model results using modern data (1979–2013), Neff and Bertler (2015) found that Patagonian dust dominates the Atlantic and Indian sectors of the Southern Ocean and that New Zealand, like Australia, is a potentially significant dust source to the Pacific sector of the Southern Ocean (Figure S1). The largest dust emissions are often simulated from Australia and Patagonia (Albani et al., 2012; Ginoux et al., 2001; Li et al., 2008; Wagener et al., 2008). Joussaume (1993), and Li et al. (2008) argued that Australia is the largest Southern Hemisphere dust source, and geochemical data indicate that Australian dust has been deposited in Antarctica (De Deckker et al., 2010; Revel-Rolland et al., 2006; Vallelonga et al., 2002). Other authors have argued that Patagonia is the dominant Southern Hemisphere dust source (Delmonte et al., 2004; Grousset et al., 1992; McConnell et al., 2007). Furthermore, Patagonia possibly contributed more dust during glacial periods due to the expanded continental shelf around the Falkland Plateau during glacial sea level lowstands (Basile et al., 1997; Lunt & Valdes, 2002; Walter et al., 2000).

There is a lack of consensus between observations and model simulations about the relative importance of these dust sources in terms of temporal and spatial dust production variations. This produces major uncertainties and gaps in understanding of the response and role of dust in global climate change, particularly from Southern Hemisphere dust sources, which limits modeling of the role of dust in climate change (Li et al., 2008). In a review of airborne dust, global climate, and ocean biogeochemistry, Maher et al. (2010) concluded that much of the Southern Hemisphere is severely under-represented with respect to knowledge of dust inputs for both terrestrial and marine settings and that Southern Ocean data are sparse. We here present grain-size and high-resolution scanning X-ray fluorescence (XRF) records for a marine sediment core from east of New Zealand to investigate potential dust inputs from New Zealand into the Southern Ocean over several G-IG cycles.

2. Methods

We studied piston core PS75/100-4 (Figure 1; 45°45.41′S, 177°8.93′E; 2,498 m water depth; 14.77 m in length). This core was retrieved during RV *Polarstern* cruise ANT-XXVI/2 in 2010 from the southern Chatham Rise, east of South Island, New Zealand (Gersonde, 2011).

2.1. XRF Scanning Count

Continuous U-channel samples (2 × 2 cm square cross-section and length from 50 to 100 cm; Weeks et al. [1993]) were obtained from the archive halves of the core and were subjected to XRF core scanning using an Avaatech XRF scanner at the Australian National University (ANU) at 5-mm stratigraphic intervals (corresponding to sampling at an average ~140-years interval) with a down-core slit size of 5 mm and a counting time of 30 s per position. U-channel samples were covered with Ultrafine film and were measured at 10 kV with a 0.5 mA current and no filter, then at 30 kV and 0.2 mA with a thin Pd filter, and finally at 50 kV with a 0.5 mA current and Cu filter.

2.2. Elemental Concentrations

Further quantitative elemental analysis was undertaken to convert the high-resolution XRF scanning resolution records to elemental mass concentrations. A total of 39 discrete samples (average ~40 cm sampling interval) from archive core halves were divided into two groups and were measured using a Jena Plasma Quant inductively coupled plasma mass spectrometer (ICP-MS) at the Guangzhou Tuoyan Testing Technology Co., Ltd., and using an ICP optical emission spectrometer (ICP-OES, Agilent 720) at the Guangzhou Institute of Geochemistry, Chinese Academy of Sciences (CAS), respectively. For trace element measurements, ~0.05 g of powdered sample was placed in a laboratory-made PTFE bomb (Qi et al., 2000), and 0.6 ml of HF and 3 ml of HNO_3 were added. The sealed bombs were then placed in an electric oven and heated to 185°C for about 36 h. After cooling, the bombs were heated on a hot plate to evaporate and dry. Rh (200 ng) was added as an internal standard, and then 2 ml of HNO_3 and 4 ml of de-ionized water were added. The bomb was again sealed and placed in an oven at 135 °C for about 5 h to dissolve the residue. ICP-MS analytical accuracy is estimated to be better than 5%–10% for Rb, Sr, Zr, Ba, and Th in this study. For major element measurements, the sample pretreatment procedure is the same as for trace elements measured by ICP-OES. Analytical precisions are estimated to be better than 2% for Al, Si, K, Ca, Ti, Mn, and Fe in this study. Additional major element geochemical fingerprinting of volcanic glass shards was undertaken using a JEOL JXA-8230 Electron Probe Microanalyser housed at Victoria University of Wellington, New Zealand, using the analytical procedures described by Rees et al. (2019).

2.3. Grain Size Distributions

Powder samples were collected for grain size analyses at 10-cm sampling intervals. All samples ($n = 156$, including 8 duplicates) were treated in a water bath with excess 15% H_2O_2 at 60 °C for 2 h to remove organic matter and then with excess 10% CH_3COOH at 60°C for 2 h to remove carbonate. The sediment solution was then rinsed and centrifuged until near-neutral pH was reached, and was then treated with 2M Na_2CO_3 at 85°C in a water bath for 5 h to remove biogenic opal (see McCave et al. [1995]). Modern Bounty Trough and Chatham Rise sediments generally contain low opaline silica concentrations of <5% (Thiede et al., 1997). To confirm the removal efficiency of biogenic silica, smear slides from two samples from core depths of ~3 and 12 m were examined under optical micoscope before and after alkali treatment. Finally, the sample solution was deflocculated in a 5% Calgon solution and was ultrasonicated for 1 min before measurement. Measurements were made three times for each sample using a Malvern Mastersizer 2000 with Hydro MU at the Key Laboratory of Ocean and Marginal Sea Geology, CAS. An average spectrum of the three measurements for each sample was obtained to represent the respective grain size distributions. Duplicate analyses of eight pairs of sister samples demonstrated the reproducibility of grain size distributions.

2.4. Age Model

The age model for the uppermost part of core PS75/100-4 (from the top to ~33 ka) is supported by 11 ^{14}C ages from Ronge et al. [2016]; data available at Pangaea: https://doi.org/10.1594/PANGAEA.861425). To develop an age model for the 33–340 ka interval, we tuned our highly resolved scanning XRF Sr record to another scanning XRF Sr record from nearby core MD97-2120 (Ronge et al., 2016; data available at: https://doi.pangaea.de/10.1594/PANGAEA.877303) (Figure 2) using the QAnalySeries software (Kotov & Pälike, 2018) (this is an upgraded version of the AnalySeries software of Paillard et al. [1996]). The core sites are located close to each other in the Bounty Trough (Figure 1), so we assume that Sr variations in cores PS75/100-4 and MD97-2120 evolved approximately parallel to each other. However, the MD97-2120 Sr record does not extend to older than ~340 ka (Pahnke et al., 2003), so we tuned the oldest section of our PS75/100-4 Sr record to the Antarctic EPICA Dome C (EDC) ice core on its AICC2012 age scale (Bazin et al., 2013; Jouzel et al., 2007; Lambert et al., 2008; Veres et al., 2013), based on graphic correlation between EDC δD and both Sr records over major transitions (Figure 2). We avoid over-tuning by limiting our tie points to Termination IV, the MIS 10/11 boundary, and the MIS 11 peak. We note, however, that the oldest tie point at 407 ka is less well constrained, owing to the increasing Sr trend toward the base of the core. The base of the core is correlated to the MIS11 maximum in the EDC δD profile, which corresponds to an age of ~407 ka. This could be an over-estimate, although it is consistent with a maximum age of ≤0.44 Ma reported

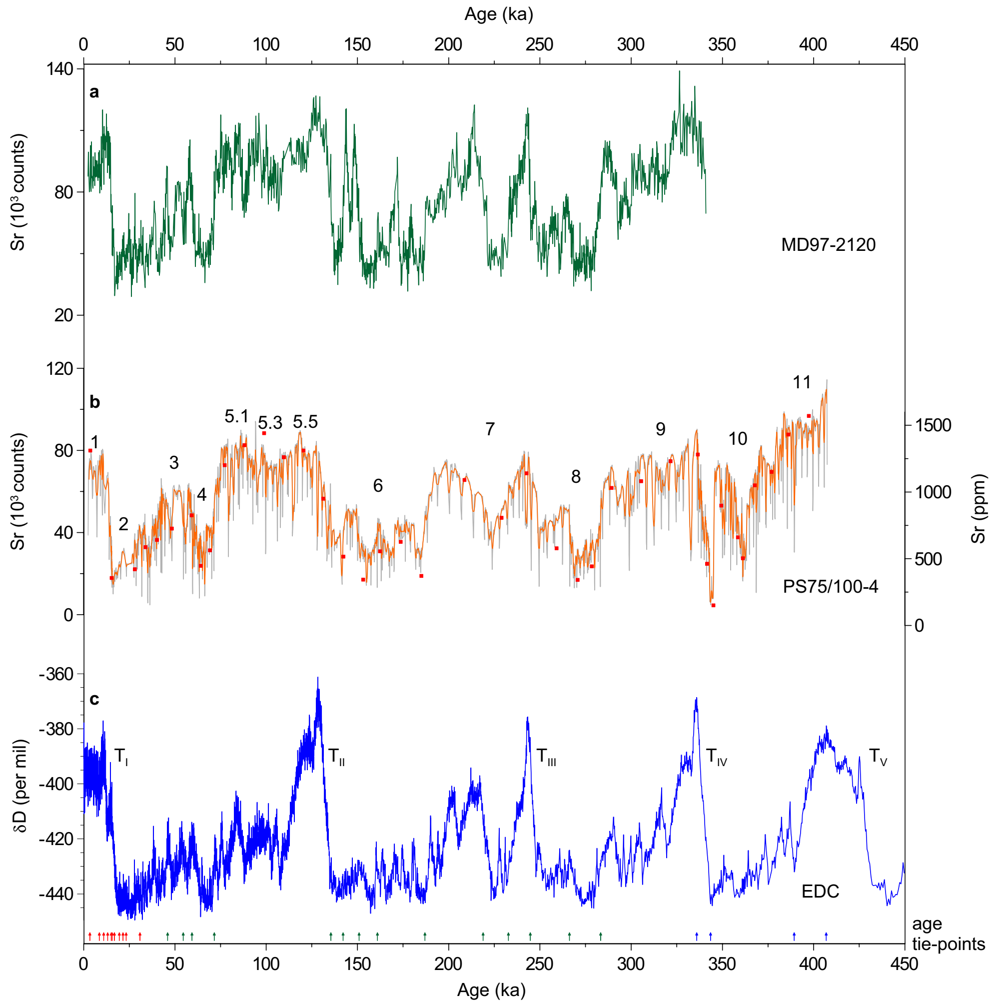

Figure 2. Tuning of core PS75/100-4 to core MD97-2120 and to EPICA Dome C (EDC). (a) Scanning XRF Sr record from core MD97-2120 (Ronge et al., 2016; data are available from https://doi.pangaea.de/10.1594/PANGAEA.877303), which is used as a tuning target from ~40 to 280 ka. (b) Scanning XRF Sr record and ICP-OES derived Sr content from core PS75/100-4 (this study; gray for raw data, and orange after 5-point smoothing from XRF scanning data; red dots for Sr contents), and (c) the Antarctic EDC ice core δD record (Bazin et al., 2013; Veres et al., 2013; data are available at: https://doi.pangaea.de/10.1594/PANGAEA.824894), which is used as a tuning target for the base of core PS75/100-4. Age control points are indicated along the lower axis: ^{14}C ages (red; Ronge et al., 2016), and tie-points to core MD97-2120 (green) and to EDC (blue) were transferred to core PS75/100-4. Marine isotope stages (MISs) are indicated by numbers in (b), and terminations are radiolabeled from T_I to T_V in (c).

for core PS75/100-4 based on shipboard calcareous nannofossil observations (Figure 7.6.1, Table 7.6.1 in Gersonde [2011]). All age-depth points are listed in Table 1.

The average sedimentation rate (SR) for core PS75/100-4 is approximately 3.6 cm/kyr, and SRs were further calculated for each MIS using age/depth points for each MIS boundary (Figure 3). Glacial stages MIS 6 and 8 have higher SRs than neighboring interglacial stages MIS 7 and 9. The average SR for MIS 2–4 is comparatively much higher, while the SR was also high in MIS 5. MIS 10 has an apparently high SR because two volcanic ash layers occur in the 12–13 m depth interval (at 12.14–12.26 m and 12.93–12.95 m). Super-eruptions from the Taupo Volcanic Zone (TVZ), North Island, New Zealand, produced significant ash thicknesses both onshore on the nearby Chatham Islands and in marine sediments from Chatham Rise (Carter et al., 1995; Holt et al., 2010; Vandergoes et al., 2013). The two largest and most widespread of these were the Kawakawa Tephra (which erupted in MIS2) and the Rangitawa Tephra, which erupted toward the end of MIS10 (Carter et al., 1995; Holt et al., 2010; Kohn et al., 1992; Pillans et al, 1993, 1996). Electron probe

Table 1
Age Control Points for Core PS75/100-4

Depth (m)	Age (ka)	Age control points	References
0.02	3.41	0.02–1.03 m: ^{14}C ages	Ronge et al. (2016)
0.12	8.56		
0.24	10.98		
0.26	13.16		
0.36	15.15		
0.54	15.63		
0.62	16.87		
0.68	19.51		
0.72	21.59		
0.74	23.26		
1.03	30.83		
2.00	46.02	2.00–10.28 m: Sr tuned to Sr of MD97-2120	Ronge et al. (2016)
2.11	54.58		
2.45	59.40		
3.42	71.62		
5.78	135.49		
6.02	142.16		
6.33	150.96		
6.78	160.97		
7.70	187.02		
8.18	218.86		
8.52	232.74		
8.89	244.79		
9.39	266.21		
10.28	283.29		
11.58	335.97	11.58–14.74 m: Sr tuned to δD of EDC	Bazin et al. (2013); Veres et al. (2013)
12.17	343.50		
14.17	389.39		
14.74	406.92		

microanalyses on the ash layer at 12.93–12.95 m indicate that it represents the Rangitawa Tephra (Kohn et al., 1992), and not the Kawakawa Tephra (Figure S2; Table S1), which further supports our age model for core PS75/100-4.

3. Results

3.1. Grain Size Variations

Grain size analyses reveal that the sediment consists predominantly of very fine to coarse silt on the scale of Blott and Pye (2001). Most of the samples analyzed here have similar grain size distributions, with median grain sizes (Md) of ~10–20 μm, which differ from those of sediments in neighboring areas, such as from New Zealand loess with Md of ~8–40 μm, and Tasman Sea sediments with Md of ~3–6 μm (Figure 4a). End-member (EM) modeling of the grain size data following Paterson and Heslop (2015) for core PS75/100-4 suggests that a three-EM model provides an optimal fit that accounts for >99% of data variance with <5° angular deviation (Figures S3 and 4b). Down-core variations of the three EMs have distinct stratigraphic

10.1029/2020PA003949

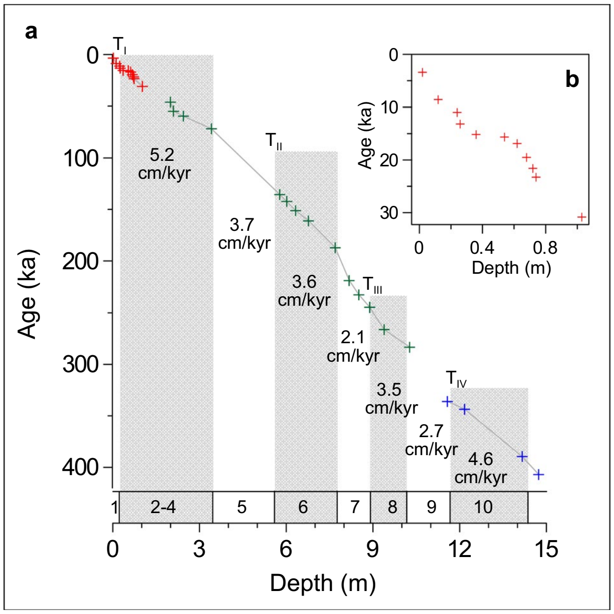

Figure 3. Age-depth model for core PS75/100-4. (a) The 11 red crosses represent ^{14}C dates for the upper 1.03 m of the core (inset in [b]) from Ronge et al. (2016); 14 green and 4 blue crosses represent age tie-points from core MD97-2120 (Pahnke et al., 2003; Ronge et al., 2016) and the Antarctic EDC ice core δD record (Bazin et al., 2013; Veres et al., 2013), respectively. Age points at MIS boundaries are used to calculate average sedimentation rates for each glacial/interglacial stage. Gray shading indicates even-numbered (glacial) MISs. Generally, glacial stages have higher mean sedimentation rates than surrounding interglacials (odd-numbered MISs); MIS 10 has a relatively high apparent sedimentation rate because two volcanic ash layers occur in the 12–13 m interval.

patterns over G-IG timescales (Figures 4c–4e). Results for conventional grain size parameters are also shown in Figures 5a–5d and 6.

Bulk sediment Md undergoes small size variations throughout the core, except within two peaks in the 12–13 m interval, with ages of ∼344 ka and 361–363 ka (Figure 5a), which are due to volcanic ash layers. Apart from these peaks, Md values generally vary between 8 and 21 μm (∼98% of samples), within the medium to coarse silt range. Sand and clay contents have inverse trends on G-IG timescales throughout the core (Figures 5b and 5d). Glacial and interglacial stages generally have contrasting clay contents, with interglacials generally preserving slightly smaller clay proportions (Figure 5d). Silt is the dominant component with an ∼89% average content (Figure 5c). As shown in Figure 6b, the four fine size fractions generally have a similar pattern over G-IG timescales, with relatively high contents in glacials and low contents in interglacials. The four fine size fractions account for ∼25%–75% of samples, with a ∼57.3% average throughout the core. In contrast, except for the coarse silt fraction (16–31 μm), the coarser fractions (Figure 6a) have an inverse G-IG variation pattern. EM variations (Figures 4c–4e) are consistent with these patterns (Figure 6), which demonstrates the comparability of results from different approaches. EM1 has the same variations as the three fine fractions, while EM2 is more similar to the average signal. Coarse EM3 (Figure 4e) appears to be controlled by coarse volcanic ash shards in a few samples (outlier gray curves in Figure 4a), along with the very coarse silt and sand components (Figure 6a).

Two sortable silt size parameters, SS% and $\overline{SS}$, are defined as the percentage of the 10–63 μm fraction within the <63 μm fraction and the 10–63 μm geometric mean grain size, respectively, and are used to evaluate sediment sorting by paleocurrents (Bianchi et al., 1999; McCave et al., 1995; McCave & Andrews, 2019; McCave & Hall, 2006). These parameters can provide an estimate of flow speed along a current pathway if measured for a series of core sites (McCave, 2020; McCave et al., 2017). Profiles of these parameters have similar variations throughout core PS75/100-4; both have higher values during interglacials than within adjacent glacials (Figures 5e and 5f). However, the G-IG contrast is not prominent compared to the very coarse silt and sand fractions (Figure 6a). Linear correlation between SS% and $\overline{SS}$ ($r = 0.86$; Figure 7a) indicates a well-sorted sediment (McCave et al., 1995, 2017; McCave & Andrews, 2019; McCave & Hall, 2006). Two silt peaks near the bottom of the core (Figures 5e and 5f) suggest that the tephra were not sorted by ocean currents. Interglacial $\overline{SS}$ values generally decrease toward the core top (Figure 5f). IRD% is the percentage of ice-rafted detritus estimated from the >240 μm to >550 μm fractions (McCave & Andrews, 2019). Both fractions are small (<2%), with episodic jumps during interglacials (Figure 5g). Lack of correlation between $\overline{SS}$ and coarse IRD (Figures 7b and 7c) indicates that coarse IRD was not sorted by bottom currents (McCave & Andrews, 2019) and few coarse grains greater than 240 or 550 μm are present in the core.

3.2. Geochemical Variations

Semi-quantitative (scanning XRF) elemental records from core PS75/100-4 are shown in Figure S4, along with weight concentration values from geochemical analyses of discrete samples for 11 of 13 elements. Linear relationships exist for the XRF scanning counts and respective elemental concentrations (Figure S5). Scanning XRF counts were converted into element concentrations using a multivariate log-ratio calibration (MLC), following Weltje et al. (2015). Cl and Br XRF counts were not calibrated because they are not detectable using ICP-OES and ICP-MS analyses in the instruments used for this study. Ca and Fe counts are an order of magnitude higher than those of the other elements and dominate interglacial and glacial periods, respectively. Al, Si, K, Ti, Mn, Rb, and Zr, and to a lesser extent Ba, have similar down-core variations as Fe.

10.1029/2020PA003949

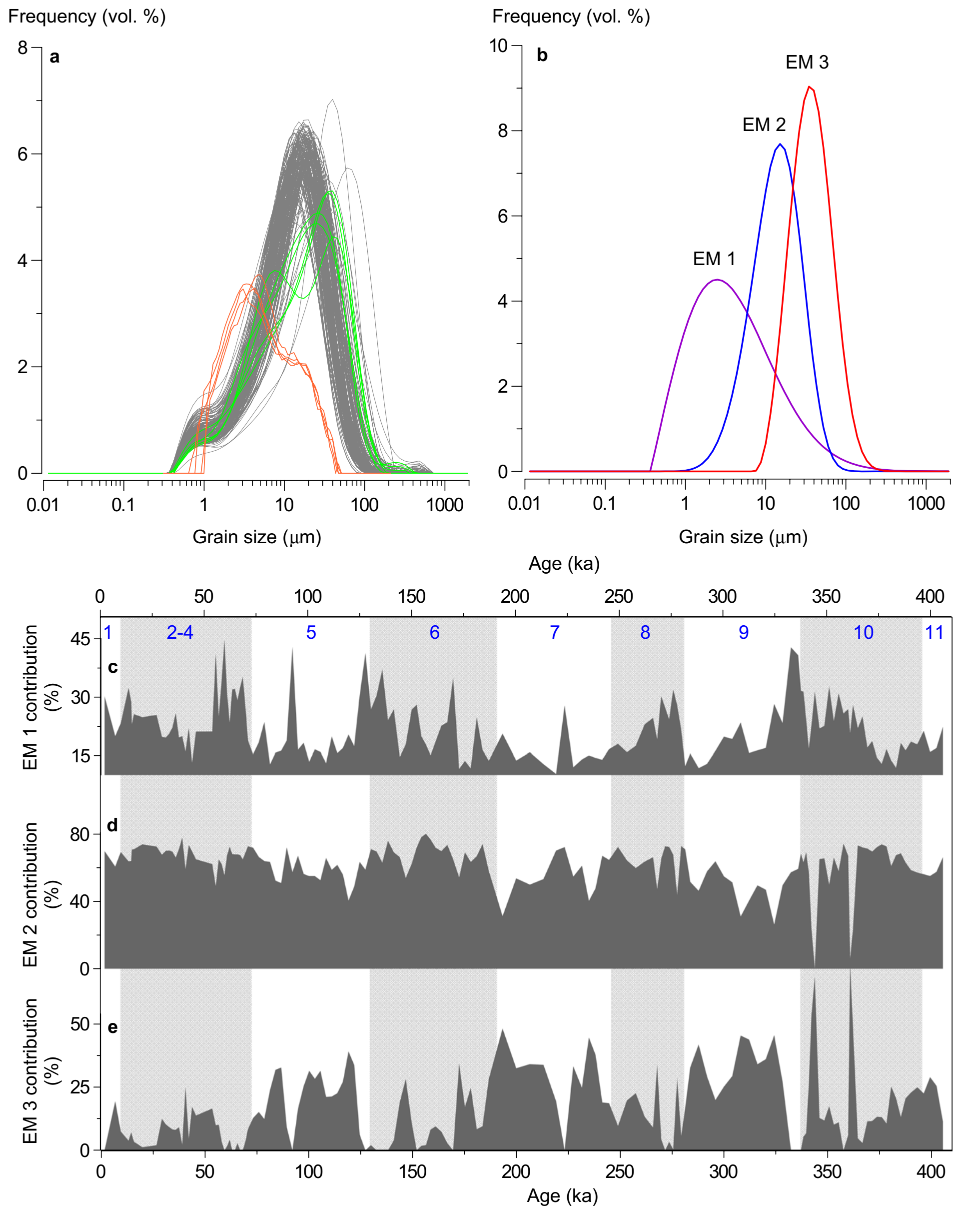

Figure 4. Sediment grain size distributions and their end-member modeling results for core PS75/100-4, compared with New Zealand loess, and Tasman Sea sediments. (a) Results for 148 samples (gray) from core PS75/100-4 (this study), five representative loess samples (green) from Dashing Rocks loess, New Zealand (Ma et al., 2013), and four samples (orange) from Tasman Sea core E26.1 (Hesse & McTainsh, 1999). (b) Three grain size components from core PS75/100-4 were unmixed using the AnalySize software (version 1.2.1) of Paterson and Heslop (2015); with additional modeling result comparisons shown in Figure S3. (c)–(e) Down-core variations of the three end-member contributions to the entire grain size data set.

In contrast, Ca and Sr dominate in interglacials and interstadials (in calcareous oozes). These observations are confirmed by principal component analysis (PCA) (Table 2; Figure 8). Principal component 1 (PC1) accounts for 74% of the data variance and represents detrital versus biogenic inputs. These geochemical patterns (Figure 8) are consistent with sediment color and lithology, where glacial intervals are generally dark gray and rich in terrigenous sediment, while interglacial sediments are light gray and enriched in biogenic carbonate. Such variations also characterize other Southwest Pacific sites, where alternations are documented between predominant calcareous oozes during interglacials and siliceous oozes or siliciclastic

10.1029/2020PA003949

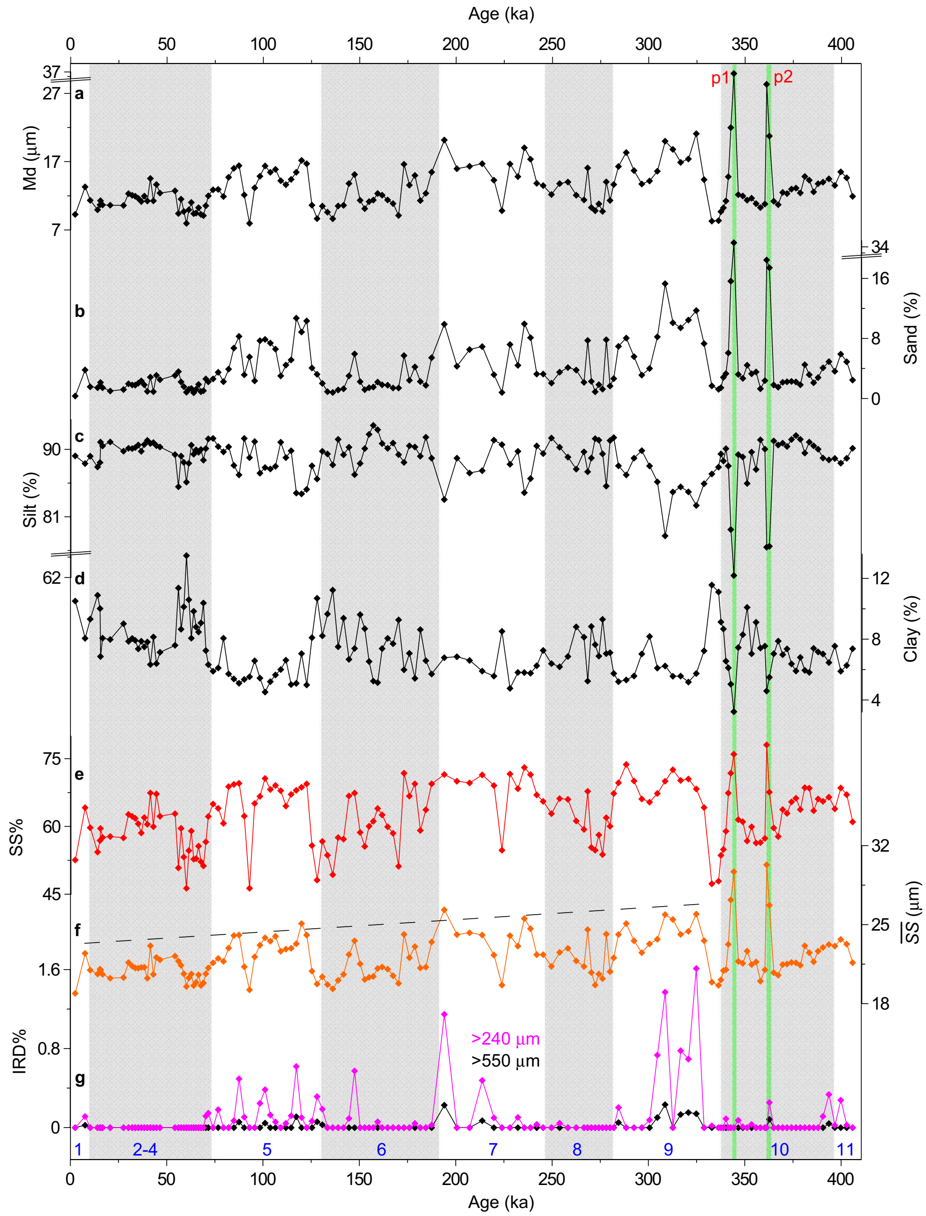

Figure 5. Grain size variations for core PS75/100-4. Two grain size peaks in a-b and through e-g are marked as p1-p2 in green vertical bars. Shown are the records of: (a) Md, the median grain size; (b) sand; (c) silt; (d) clay; (e) SS%; and (f) $\overline{SS}$, sortable silt grain-size parameters (see text); and (g) IRD%, the percentage of ice rafted detritus. Sand, silt, and clay components represent the >63 μm, 2–63 μm, and <2 μm sediment fractions, respectively (Blott & Pye, 2001). A dashed line along the $\overline{SS}$ profile indicates a general decreasing trend toward the core top mainly for interglacials. A broken scale is used in the *y*-axes in (a–c) to better reveal whole-core variations by suppressing data points with extreme high/low values. Results for 148 analyses are shown in each profile for (a–g).

sediments during glacial intervals (e.g., Carter et al., 2000; Carter & Gammon, 2004; Lamy et al., 2014; Nelson et al., 1985).

Ca and Sr also contribute to PC2 (18% of the data set variance), although Cl and Br are dominant and tend to covary (Table 2; Figure 8b). Cl in deep-sea sediments is related to Na, and both can be enriched in marine sediments because of their presence in interstitial sea water (e.g., Turekian & Wedepohl, 1961), which is related to porosity. Similarly, Cl is used to infer water content in XRF-scanned sediment cores (Hennekam & De Lange, 2012), where Cl reflects both interstitial water and that trapped beneath the scanning XRF film.

10.1029/2020PA003949

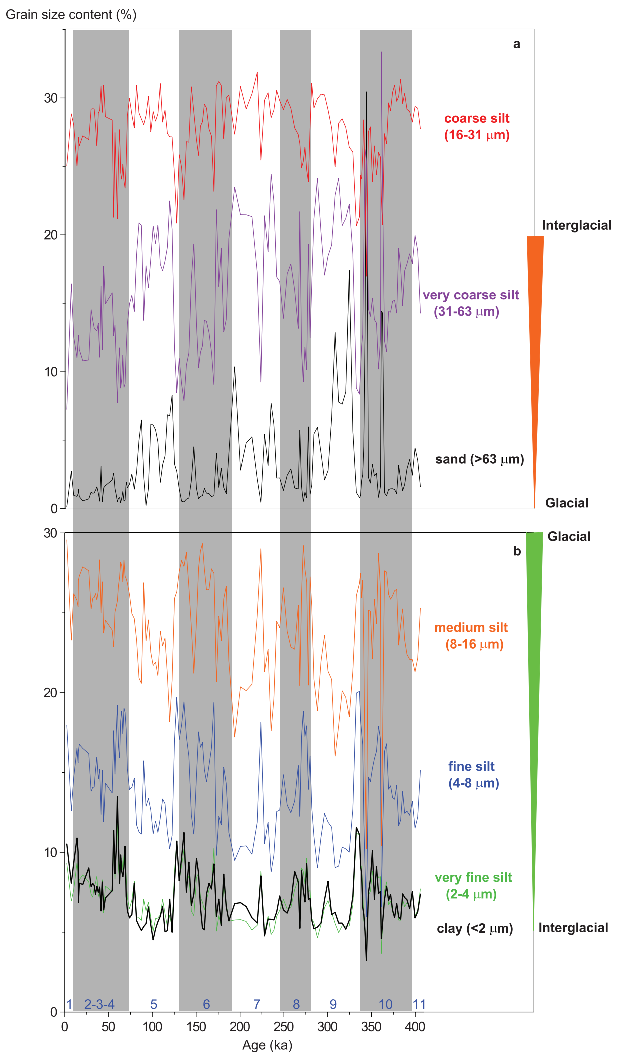

Figure 6. Variations of grain size fractions with age for core PS75/100-4. For the 2–63 μm grain size interval (i.e., silt content in Figure 5), five fractions are shown: very fine, fine, medium, coarse, and very coarse silt following the terminology of Blott and Pye (2001). Results for 148 analyses are shown in each profile in (a and b).

Br can be an effective indicator of total organic carbon content in marine sediments (e.g., Hodell et al., 2013; Ziegler et al., 2008) and can also track porosity changes if they relate to organic content changes (Thomson et al., 2006). PC2 may, therefore, be a mixed productivity/porosity signal. Ba also contributes to PC2 (to a lesser extent and contributes equally to PC1; Table 2) and is a commonly used marine paleoproductivity proxy (Dymond et al., 1992). This lends support to an export productivity signal within PC2, but additional proxies would need to be measured to reveal an unambiguous record of past productivity changes at this site, which is not a major objective of this study. We also note that our PC2, Cl, and Br records lack a clear G-IG signal, in contrast to all other elements.

3.3. Sedimentation Variation

Late Quaternary sediment has accumulated in the Bounty Trough with a generally decreasing SR from west to east. At the head of the trough, offshore of the Canterbury region, regional SRs recorded in marine sediment cores fluctuate greatly, and are as high as ~37 cm/kyr since 440 ka (Ding et al., 2017). To the east, core MD97-2120 records SRs that fluctuate between 15.5 cm/kyr during glacials and 6 cm/kyr during interglacials (Pahnke et al., 2003), which is much higher than those in core PS75/100-4 (Figure 3). ODP Site 1122 has higher SRs, probably because it is located on the abyssal Bounty Fan, which receives material transported through the long Bounty Channel (Carter et al., 1999; Figure 1). These observations indicate a much-diminished fluvial sediment supply to the site of core PS75/100-4 compared to sites located closer to shore and along the Bounty Channel. For example, the Rangitawa Tephra (~350 ka) occurs at a down-core depth of ~140 m at Site 1122 (Carter et al., 1999), which is much deeper than in core PS75/100-4 (12.93–12.95 m).

3.4. Lithogenic Flux Calibration

Mass accumulation rate (MAR) results for Fe and lithogenic contents can be calculated as follows (e.g., Carter et al., 2000):

MAR = mass concentration of a component (in dry bulk sediment) × SR × DBD, where DBD is the dry bulk density, which was determined following Dadey et al. (1992) using processed fractional porosity (FP) data from direct shipboard measurement of fresh sediments. A standard quartz density value (2.65 g/cm^3) is used for "grain density":

$$\text{DBD} = (1\text{-FP}) \times \text{grain density}.$$

The MAR calculation relies on a good linear relationship between XRF scanning results and elemental contents (Figure S5). ^{232}This used as a normalizer to quantify lithogenic contents by assuming the average concentration (~10.7 ppm) of upper continental crust (Taylor et al., 1995). This approach has been adopted widely to approximate lithogenic fluxes in deep-sea sediments (e.g., Lamy et al., 2014; Martínez-García et al., 2009). Other normalizers can also be used. For example, ^{230}Th could be a better normalizer (to ~330 ka, due to the half-life of ^{230}Th; Costa et al. [2020]), but such data are not available. We compare here reconstructed MARs with other relevant records. Our ^{232}Th lithogenic and Fe weight contents have a linear relationship before (r = 0.71) and after (r = 0.98) removal of outliers (Figure 9). Based on this relationship, a high-resolution lithogenic MAR record is determined for core PS75/100-4 (Figure 10), which has a wide of range of values (~0.01–0.69 g/cm^2/kyr), with an average of ~0.20 g/cm^2/kyr. Glacial averages are approximately 3–4 times larger than in interglacials. This prominent difference is unlikely to be ascribed to the sorting effect of paleocurrent circulation during interglacials for which $\overline{SS}$ indicates much enhanced flow speeds compared to glacials (Figure 5f) because there is no evident difference of correlations between the

10.1029/2020PA003949

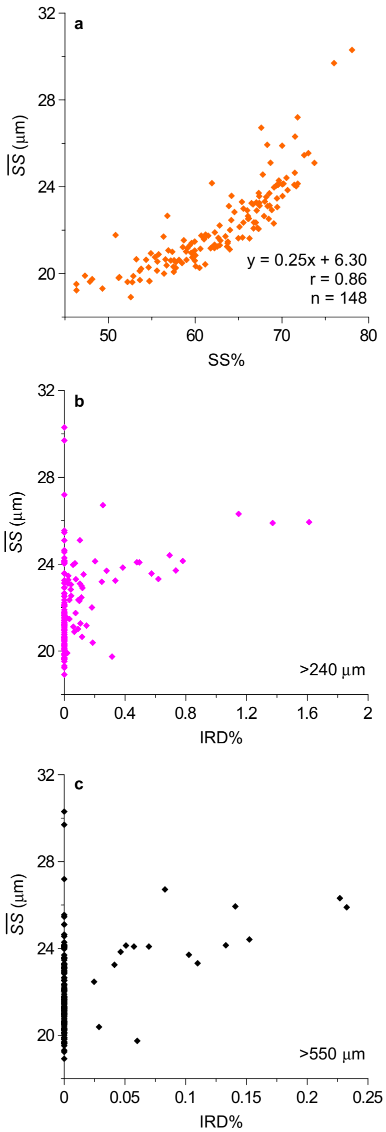

Figure 7. Plots of (a) $\overline{SS}$ versus SS%, (b) $\overline{SS}$ versus IRD% (>240 µm), and (c) $\overline{SS}$ versus IRD% (>550 µm).

two sortable size proxes on G-IG timescales (Figure 7a). The record follows the variation pattern of PC1 (Figure 8) and has distinct similarities with Antarctic and Southern Ocean dust records (Figure 10) over G-IG timescales. The marine sediment records generally have the same order of magnitude Fe contents and lithogenic MAR. Together, these features indicate large-scale climatic modulation of sedimentation in time and space over G-IG timescales.

4. Discussion

4.1. Riverine Inputs to the Core Site

Sediment transport through the Otago and South Canterbury regions of South Island, New Zealand, by large eastward-draining rivers generates a high proportion of suspended load that is abraded to silt and finer sizes (Adams, 1980; Carter et al., 2000; Gibb & Adams, 1982; Land et al., 2010; Nelson et al., 1985). This sediment is supplied to submarine channels and into the path of the deep western boundary current that then transports sediment along southern Chatham Rise (Carter et al., 1996; Carter & Wilkin, 1999, Figure 1). Carter et al. (1996) found that all submarine channels offshore of eastern New Zealand were active and emptied into the Pacific deep western boundary current during glacials (Figure 1). The broader continental shelf width during glacial sea level low stands (Figures 1a and 1b) is likely to have assisted fine riverine sediment delivery, and, thus, to have enhanced offshore deep-water mud deposition (Nelson et al., 1985).

Grain size analysis reveals a current-sorted silt fraction in core PS75/100-4 (Figure 7; see Section 3.1). As a proxy for evaluating flow speed variations (McCave & Hall, 2006; McCave et al., 2017), $\overline{SS}$ in core PS75/100-4 has clear G-IG contrasts over the past 410 kyr, with lower values in glacials and higher values in interglacials (Figure 10c). In contrast, ODP Site 1123, which is located northeast of Chatham Rise (Figure 1), generally has higher $\overline{SS}$ values in glacials versus interglacials over the past 1.2 million years (Hall et al., 2001). From that site, Hall et al. (2001) identified intensified deep Pacific Ocean inflow from the Southern Ocean through the Pacific deep western boundary current (DWBC), which ventilated bottom waters during Pleistocene glacials. $\overline{SS}$ values also have clear differences between the two cores; in core PS75/100-4, they range from ~19 to 30 µm with an average of ~22 µm, while for Site 1123 they range from ~12 to 19 µm with an average of ~16 µm (Figures 10c and 10d). This indicates generally stronger flow speeds at the core PS75/100-4 site over the past 410 kyr. Furthermore, the sortable silt proxy appears to have recorded a decreasing long-term flow speed over the most recent interglacials in our core (Figure 10c, this study), which is not evident at ODP Site 1123. Rather, there appears to be an increasing long-term flow speed over recent glacials (Figure 10d). The different indication from core PS75/100-4 is not likely to be a DWBC signal, which is linked to the Antarctic Circumpolar Current because core PS75/100-4 is located at a much shallower depth in Bounty Trough (Figure 1), away from the DWBC pathway (Carter et al., 1996; Carter & Wilkin, 1999). Paleoflow at these two core sites appears to have had opposite patterns on G-IG timescales over the last ~250 kyr (Figures 10c and 10d).

By analyzing short sediment cores around Chatham Rise, McCave et al. (2008) reported no clear indication of faster glacial DWBC flow as indicated at ODP 1123. Some core sites studied by McCave et al. (2008) are located above or away from DWBC pathways. For example, on the north of Chatham Rise core CHAT 16K (Figure 1) seems to have recorded relatively faster flow during interglacials since MIS 6 (Figure 12 in McCave et al., 2008), which provides a similar indication as our $\overline{SS}$ records.

10.1029/2020PA003949

Table 2
Results of a Standardized principal Component Analysis (PCA) on the Scanning XRF Dataset for Core PS75/100-4

	PC1	PC2
Al	0.32	0.07
Si	0.31	0.1
Cl	−0.07	0.62
K	0.32	0.04
Ca	−0.27	0.34
Ti	0.32	0.02
Mn	0.31	0.01
Fe	0.31	0.01
Br	0.17	0.5
Rb	0.31	−0.04
Sr	−0.23	0.42
Zr	0.31	0.05
Ba	0.24	0.25

Two principal components are identified, PC1 and PC2, which account for 74% and 18% of the data variance, respectively. Loadings for PC1 and PC2 are listed above for the 13 elements analyzed.

4.2. Riverine versus Eolian Sources

To further distinguish between possible eolian versus fluvial inputs to core PS75/100-4, we first focus on our Fe record. It does not evidently reflect diagenetic Fe remobilization because Fe covaries with other detrital elements (Figure 8a), which implies that our Fe record is a detrital signal. As noted above, Fe in core PS75/100-4 has variable but high abundances in glacial stages and much lower abundances in interglacial stages. Furthermore, our Fe content and reconstructed lithogenic MAR records resemble the structure of dust content changes in the EDC ice core and Fe and lithogenic MAR fluctuations in subantarctic marine sediment cores from the Pacific sector of the Southern Ocean (Figures 1 and 10). Four fine sediment fractions (Figure 6b) share a similar trend on G-IG timescales. These observations suggest that the fine components (Figure 6b) in core PS75/100-4 represent an eolian dust record from Australia, New Zealand, or both, which presumably reveal a common response to westerly wind intensity (see grain-size discussion below).

Despite the observations indicated above, we cannot yet rule out a riverine source for the core PS75/100-4 Fe content. Ti/Al can be used to reconstruct eolian versus fluvial sedimentary inputs (e.g., Lourens et al., 2001) and to indicate terrigenous sediment content and grain-size variations (e.g., Peterson et al., 2000). However, Ti/Al does not undergo distinct G-IG variations in core PS75/100-4 and is of no use for this purpose (Figure S6). Additionally, a minor IRD contribution (<2%) is evident. Carter et al. (2002) found that Campbell Plateau was traversed by icebergs over the past 200 ka. Our IRD% records reveal a few jumps during interglacials (Figure 5g), when warmer climates and elevated sea levels (Figures 10a and 10b) might cause icebergs to drift to the core location, which is close to the northern limit of iceberg dispersal (Carter et al., 2002; Tournadre et al., 2016). The core location might have received IRD input; however, it has only a small coarse IRD fraction.

Particle size analysis provides an additional constraint on the sediment source in core PS75/100-4. Sediment particle size distributions at ODP Site 1119 have a similar silt-dominated (>70%) pattern as documented here for core PS75/100-4, albeit using a slightly different sample pre-treatment procedure, with a ~15% clay (<4 μm) content over the same period recorded in core PS75/100-4 (Land et al., 2010). In contrast, core PS75/100-4 samples have <4 μm content of 7.5%–27.8% (~16.2% average), which make a minor contribution of ~22.0%–27.5% (~28.2% average) to the four fine fraction components (Figure 6b). The Dashing Rocks loess in eastern South Island (Ma et al., 2013) also has similar particle size distributions as sediment from core PS75/100-4 with Md values of 10–20 μm (Figure 4a). The varying clay content with distance from South Island and the dominance of silt sizes similar to onshore eolian deposits suggest that sedimentation in core PS75/100-4 was dominated by eolian rather than marine transportation.

Both Australia and New Zealand are potential dust sources to the core location (Figure S1). Jaeschke et al. (2017) demonstrated using biomarkers that surface sediments from the Pacific sector of the Southern Ocean are indicative of Australian and New Zealand lithogenic sources with a likely eolian source. However, dust deposited in the Tasman Sea to the west of New Zealand, which was transported from inland Australia (Hesse, 1994; Hesse & McTainsh, 1999), is finer-grained than the Dashing Rocks loess and core PS75/100-4, where core E26.1 sediments have Md values of 4–6 μm (Figure 4). The SRs of bulk sediments are also clearly higher in core PS75/100-4 (Figure 3) than in Tasman Sea core E26.1 (Figure 5b in Hesse, 1994) during most glacial and interglacial periods. Furthermore, surficial seafloor sediments from east of South Island record lithogenic fluxes between 2.05 and 0.27 g/cm^2/kyr (nine locations from 44.09°S, 174.10°E to 45.76°S, 177.15°E, see Figure S7; Table 1 in Wengler et al. [2019]). For comparison, core PS75/100-4 has an average lithogenic MAR of ~0.20 g/cm^2/kyr through the past ~410 kyr, with much higher glacial (3–4 times) compared to interglacial lithogenic fluxes over the past 410 kyr. In contrast, Tasman Sea core E26.1 records dust fluxes of ~0.1 g/cm^2/kyr during interglacials and stadials (Figure 5d in Hesse [1994]). The modal coarse component diameter in core E26.1 is ~19–23 μm, which is close to that of core PS75/100-4 and New Zealand

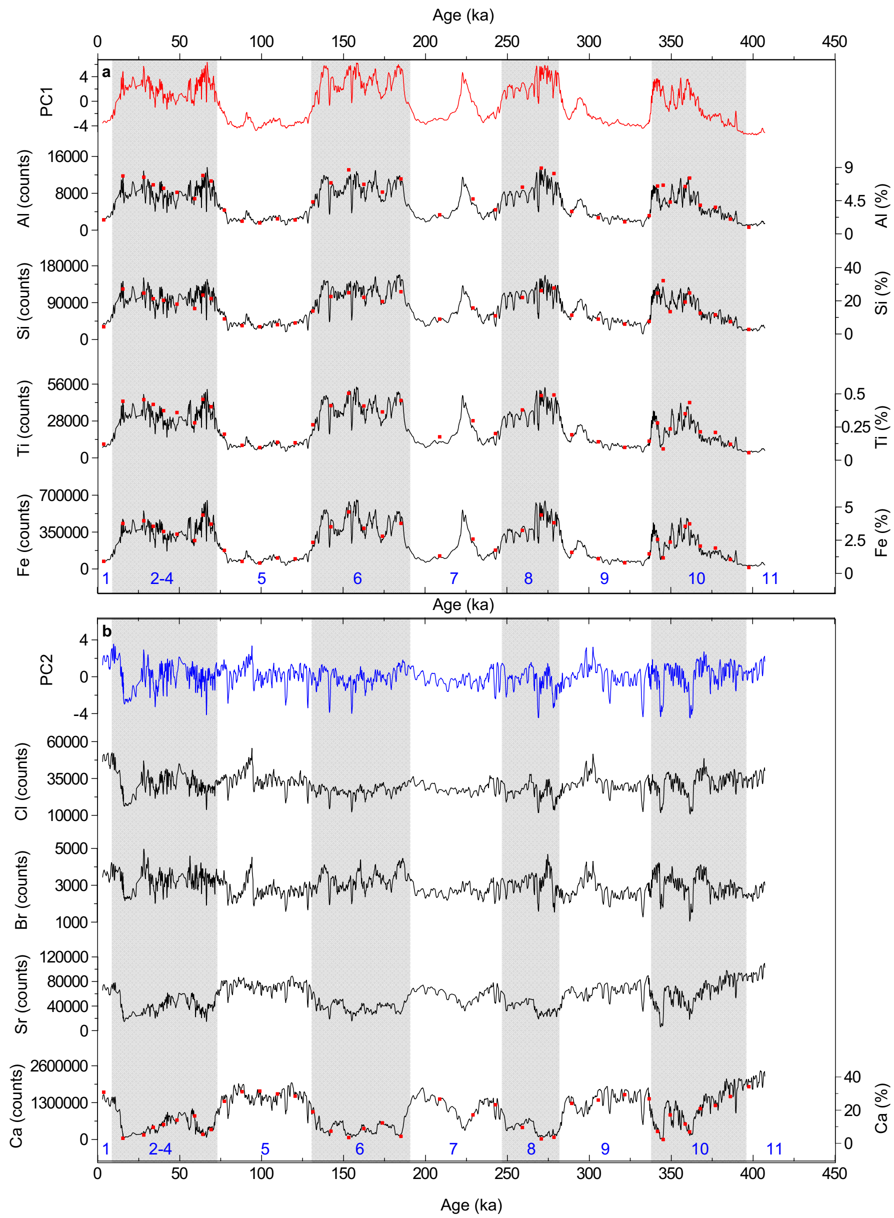

Figure 8. Down-core variations of two principal components with related element counts (5-point moving average for each) and concentrations. (a) PC1, (b) PC2. Glacial stages (gray shading) and MIS 1–11 (blue text) are indicated. Continuous lines represent XRF core scanning data and red dots represent elemental concentrations from discrete sample measurements.

loess (Figure 4). Core E26.1 is located far from New Zealand (Figure 1), although its coarse component could have a volcanic soil contribution from western North Island, New Zealand (Hesse & McTainsh, 1999). We suggest that the fine fractions indicated in Figure 6b, including the medium silt component (8–16 μm) and much of the fine silt component (4–8 μm), are dominated by New Zealand-sourced dust because their size distributions are intermediate between those of Tasman sea sediments and New Zealand loess (Figure 4a). Trudgill et al. (2020) studied sediment cores from the Southwest Pacific Ocean and suggested that a ~0.5–12.5 μm sediment component represents dust, which had higher fluxes during the last glacial maximum compared to the Holocene. This is broadly consistent with our records over G-IG timescales. Our observations suggest that core PS75/100-4 sediments were derived dominantly from a more proximal source than Australia. We, thus, exclude Australia as the source of at least the coarse-grained component in core PS75/100-4, whose source area must be New Zealand.

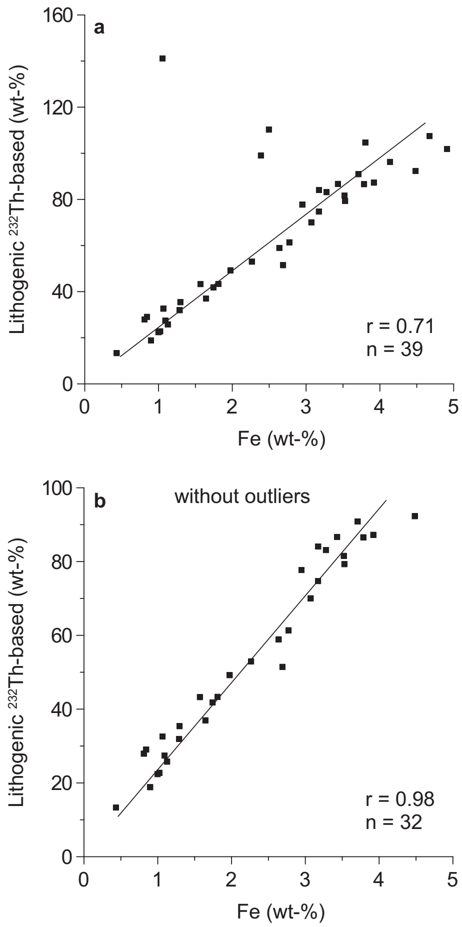

Figure 9. Linear regressions between (a), (b) Fe concentrations and ^{232}Th-based total lithogenic content. A higher regression coefficient is obtained in (b) after removal of outliers (values > 10 ppm). wt-% = weight percentage concentration.

The oldest loess in the Dashing Rocks profile is estimated to be >400 ka, while other boreholes (e.g., Darling Holes) preserve older loess (Ma et al., 2013) with ages <773 ka (Pillans, unpublished paleomagnetic results cited by Berger et al. [2001]). This implies that New Zealand has been a long-term dust source with transportation by southern mid-latitude Westerlies. Given the various lines of evidence presented here, we conclude that Fe variations in core PS76/100-4 reflect an eolian dust signal.

4.3. New Zealand as a Significant Dust Source

During the last glacial maximum, the Southern Alps, South Island, New Zealand, were glaciated by large valley glaciers (Nelson et al., 1985; Shulmeister et al., 2019), and the environment was dusty because of increased glacial, fluvial, and wind erosion of mountain ranges (Carter et al., 2000; Stewart & Neall, 1984). Glacial loess sequences were deposited in eastern South Island (Berger et al., 2001; Eden & Hammond, 2003; McCraw, 1975; Raeside, 1964), which is located beneath the Southern Hemisphere westerly maximum (Alloway et al., 2007; Li et al., 2008; Shulmeister et al., 2004). Given its position within the Roaring Forties westerly wind belt, New Zealand can contribute eolian sediment to the open ocean (Stewart & Neall, 1984; Thiede, 1979). Paleodata reveal that during glacials, Southern Hemisphere westerly winds likely intensified over an increased latitudinal range (Kohfeld et al., 2013) with shifts in latitude and intensity and divergent climatic effects on land and on the ocean (e.g., McGlone et al., 2010). Such changes will have transported dust widely from Southern Hemisphere sources, although details of shifts in intensity and position of the westerly winds on G-IG timescales remain controversial (Russell et al., 2006; Sime et al., 2013). Glaciers in the New Zealand Southern Alps advanced and retreated (e.g., Putnam et al., 2010, 2013) and northward/southward oceanic Subtropical Front shifts occurred on G-IG timescales (Figure 1). These factors likely contributed to significant dust delivery to the studied core site.

In addition to being transported to the sea, silts and clays that were deflated from extensive glacial and river outwash surfaces now mantle the landscape as loess deposits with thicknesses mostly between 1 and ~11 m in coastal eastern South Island (e.g., Berger et al., 2001; Eden & Hammond, 2003; Ma et al., 2013; McCraw, 1975; Raeside, 1964). The thickest Pleistocene loess deposits have thicknesses up to 20 m near Timaru, which overlie unconformably the 2.5 Ma Timaru basalt, on the east coast of South Island (Pillans, 2003). Such sediments would also have been deposited on the exposed continental shelf during glacial sea level low stands (Browne & Naish, 2003; Carter et al., 2000; Raeside, 1964). Nelson et al. (1985) suggested that a significant proportion of terrigenous silt in hemipelagic sediments from DSDP Site 594, which is located about halfway between core PS75/100-4 and the South Island coastline (Figure 1), would have been transported by wind from these outwash surfaces to offshore locations by prevailing and intensified westerlies. Loess deposits that formed during sea-level low stand on the exposed continental shelf would have also been eroded and transported elsewhere during subsequent sea-level transgressions. In core PS75/100-4, terrestrial inputs dominate sediment geochemical signals (Table 2; Figure 8).

Antarctic ice core records (Lambert et al., 2008; Petit et al., 1990) can help to elucidate Southern Hemisphere eolian dust transportation history. We here interpret our record (Figure 10) as a dust-dominated signal because the overall pattern of dust content variations is similar among dust records from Antarctic ice (Lambert et al., 2008) and in sediment cores (Lamy et al., 2014; Martínez-García et al., 2009) from different parts of the Southern Ocean (Figure 10). Different sectors of the Southern Ocean have similar dust or dust-dominated records, which suggests that dust generation from different regions and/or dust deposition

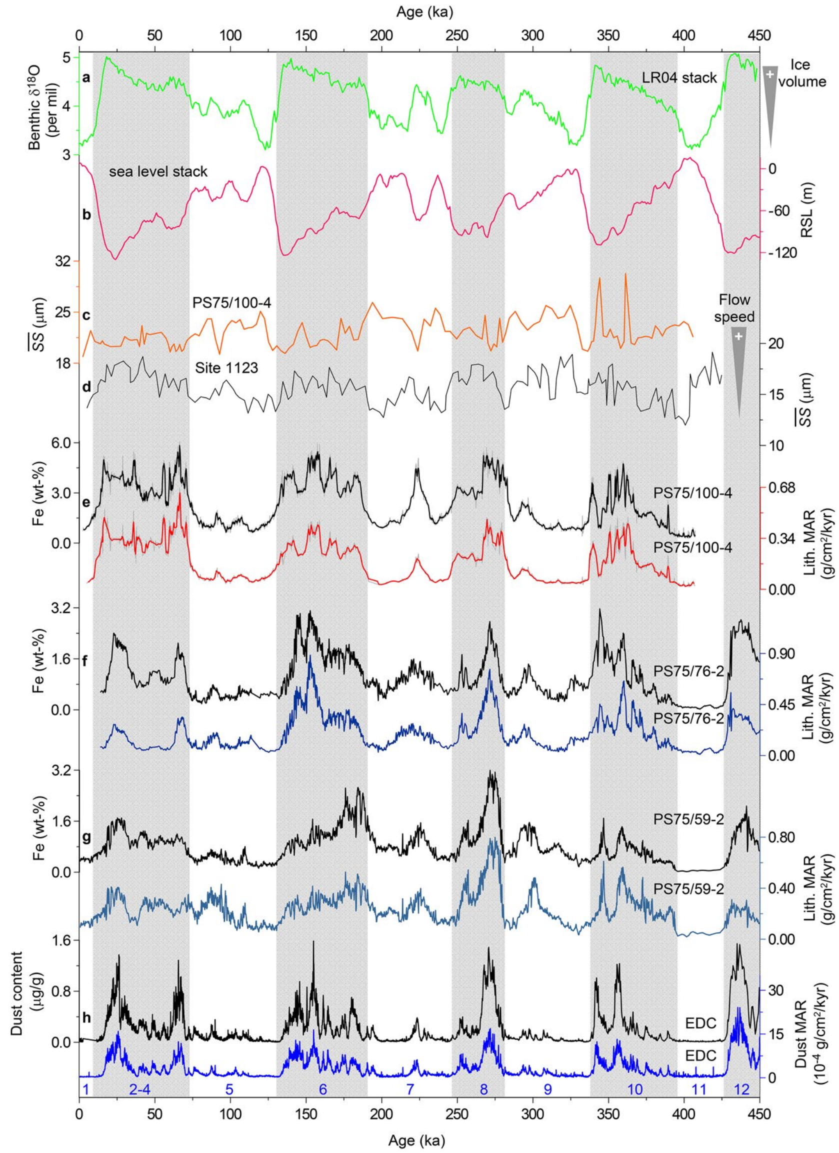

Figure 10. Core PS75/100-4 results compared with other climatic proxy records. (a) Global stack of benthic $\delta^{18}O$ (Lisiecki & Raymo, 2005), (b) global stack of relative sea level change (Spratt & Lisiecki, 2016), (c–d) $\overline{SS}$ (sortable silt mean grain size) for (c) core PS75/100-4 (this study) and (d) ODP Site 1123 (Hall et al., 2001), (e–g) Fe content and lithogenic MAR records for (e) core PS75/100-4 (this study) and (f) Southern Ocean Pacific Sector cores PS75/76-2 and (g) PS75/59-2 (Lamy et al., 2014; locations see Figure 1a), and (h) dust content (black) and MAR variations (blue) in the EDC Antarctic ice core (Lambert et al., 2008) on the AICC2012 chronology (Bazin et al., 2013; Veres et al., 2013). Data in (d) were redrawn from Figure 21 in McCave and Hall (2006), as originally published in Hall et al. (2001). Gray shading indicates glacial stages.

has common features on G-IG timescales. Terrestrial (dust-dominated) inputs to the Southern Ocean are clearly in pace with the timing and pattern of G-IG climate oscillations (Figure 10). The general similarity of dust records throughout the Southern Ocean, regardless of proximity to known dust sources, makes it increasingly important to understand the signatures associated with each significant dust source, although there are also significant differences in parts of the records (Figure 10). This makes it equally important to understand temporal and spatial differences in signatures associated with each significant dust source. The evidence provided here indicates that New Zealand is a significant and long-lived dust source to the Southwest Pacific sector of the Southern Ocean. Along with recent atmospheric trajectory model results that reveal New Zealand as a potential modern Southern Hemisphere dust source (Neff & Bertler, 2015), the dust record presented here provides a highly resolved signal to understand temporal dust variations from southern New Zealand to the Southwest Pacific Ocean. Atmospheric model simulations of volcanic ash transportation from New Zealand's North Island indicate that ash clouds from super-eruptions can be dispersed radially and swept ultimately into the polar jet so that ash can be deposited throughout the Southern Hemisphere with trace deposition in Antarctica (Dunbar et al., 2017). Thus, although New Zealand is one of several Southern Hemisphere dust sources and is a relatively small source area compared to Australia and Patagonia, the potential for extensive dispersion of any such dust source makes it important to consider all potential dust sources in dust model simulations.

We note that, based on isotopic and rare earth element data from modern seafloor sediments from east and southeast of New Zealand, Wengler et al. (2019) suggested that New Zealand can be effectively ruled out as a dust source area to the South Pacific Ocean. Their focus on seafloor sediments raises the question of whether this conclusion remains applicable during glacials given the widely reported significant dust increase during glacials compared to interglacials. From isotopic analyses of the <5 μm size fraction of mid-latitude South Pacific Ocean sediments, Struve et al. (2020) reported that during the last glacial maximum Central South America (rather than Australia) made a dominant dust contribution to the South Pacific Subantarctic Zone with possibly significant dust changes across the study area on G-IG timescales. From geochemical and isotopic analyses of the <5 μm sediment fraction from New Zealand and southern Australia, Koffman et al. (2021) reported that the South Island, New Zealand, could be a geochemically distinguishable dust source to the Pacific sector of the Southern Ocean, but not a significant contributor to East Antarctica. It is, thus, possible that dust source areas with relatively small sizes, such as New Zealand, have been under-estimated in previous studies with regard to the vast open ocean areas to which dust is transported (Grousset & Biscaye, 2005). While Australian dust has been demonstrated to reach New Zealand (Marx et al., 2005), its concentration was likely to have been small (~28.2% on average) compared to that derived from the locally dusty glacial environment, as estimated from our grain size record from core PS75/100-4.

5. Conclusions

The importance of dust as a product and agent of climate change, particularly in the Southern Ocean, makes the understanding of long-term dust emission patterns from different sources an integral part of understanding climate variability and for constraining global dust cycle models. We demonstrate here that New Zealand has likely been an important and long-lived dust source to the Southwest Pacific sector of the Southern Ocean with clear climatic control over G-IG timescales. The similarity of dust records throughout the Southern Ocean regardless of proximity to known sources makes it increasingly important to understand the signatures associated with each significant dust source over G-IG timescales. Moreover, our grain size records reveal progressively decreasing interglacial paleocurrent circulation in the studied part of Bounty Trough, south of Chatham Rise, that is possibly related to a more complex paleoceanographic sediment transportation system than was recognized previously.

Acknowledgments

We thank the crew of RV *Polarstern* for drilling the core, Dr Frank Lamy for providing access to the core samples, Dr Lizzie Ingham for sampling, Dr Ulrike Proske and Mr Andrew Higgins for assistance with pilot laboratory measurements at ANU, Dr Katharina Pahnke for conducting XRF Sr measurements on core MD97-2120, Dr. Peter Neff for providing figures for dust trajectory modeling, Profs Wen Yan, Rong Xiang, and Zhong Chen for access to laboratory instruments, and the Editor (Ursula Röhl) and two anonymous reviewers for constructive comments that helped to improve the paper. The authors acknowledge funding support from the Natural Science Foundation of Guangdong Province, China (Grant Nos. 2019A1515011488 and 2016A030313160) to Yi Wu; the Australian Research Council (ARC) through grant DP110105419 to Andrew P. Roberts and Paul P. Hesse, grant FL120100050 to Eelco J. Rohling, and grant DE190100042 to Katharine M. Grant; and the Deutsche Forschungsgemeinschaft (DFG) Priority Program SPP1158 (Grant No. RO5057/1–2) to Thomas A. Ronge and Yi Wu further acknowledges support from the Key Special Project for Introduced Talents Team of Southern Marine Science and Engineering Guangdong Laboratory (Guangzhou) (GML2019ZD0204) and the China Scholarship Council.

Data Availability Statement

New data from this study are archived in Mendeley Data and can be accessed at http://dx.doi.org/10.17632/6x969smpsn.1

References

Adams, J. (1980). Contemporary uplift and erosion of the Southern Alps, New Zealand: Summary. *Geological Society of American Bulletin*, *91*(1), 2–4. https://doi.org/10.1130/0016-7606(1980)91<2:cuaeot>2.0.co;2

Albani, S., Mahowald, N. M., Delmonte, B., Maggi, V., & Winckler, G. (2012). Comparing modeled and observed changes in mineral dust transport and deposition to Antarctica between the last glacial maximum and current climates. *Climate Dynamics*, *38*(9–10), 1731–1755. https://doi.org/10.1007/s00382-011-1139-5

Alloway, B. V., Lowe, D. J., Barrell, D. J. A., Newnham, R. M., Almond, P. C., Augustinus, P. C., et al. (2007). Toward a climate event stratigraphy for New Zealand over the past 30 000 years (NZ-INTIMATE project). *Journal of Quaternary Sciences*, *22*(1), 9–35. https://doi.org/10.1002/jqs.1079

An, Z., Kukla, G., Porter, S. C., & Xiao, J. (1991). Late Quaternary dust flow on the Chinese Loess Plateau. *Catena*, *18*(2), 125–132. https://doi.org/10.1016/0341-8162(91)90012-m

Basile, I., Grousset, F. E., Revel, M., Petit, J. R., Biscaye, P. E., & Barkov, N. I. (1997). Patagonian origin of glacial dust deposited in East Antarctica (Vostok and Dome C) during glacial stages 2, 4 and 6. *Earth and Planetary Science Letters*, *146*(3–4), 573–589. https://doi.org/10.1016/s0012-821x(96)00255-5

Bazin, L., Landais, A., Lemieux-Dudon, B., Toyé Mahamadou Kele, H., Veres, D., Parrenin, F., et al. (2013). An optimized multi-proxy, multi-site Antarctic ice and gas orbital chronology (AICC2012): 120-800 ka. *Climate of the Past*, *9*, 1715–1731. https://doi.org/10.5194/cp-9-1715-2013

Berger, G. W., Pillans, B. J., & Tonkin, P. J. (2001). Luminescence chronology of loess-paleosol sequences from Canterbury, South Island, New Zealand. *New Zealand Journal of Geology and Geophysics*, *44*, 501–516. https://doi.org/10.1080/00288306.2001.9514952

Bianchi, G. G., Hall, I. R., McCave, I. N., & Joseph, L. (1999). Measurement of the sortable silt current speed proxy using the Sedigraph 5100 and Coulter Multisizer IIe: Precision and accuracy. *Sedimentology*, *46*, 1001–1014. https://doi.org/10.1046/j.1365-3091.1999.00256.x

Blott, S. J., & Pye, K. (2001). Gradistat: A grain size distribution and statistics package for the analysis of unconsolidated sediments. *Earth Surface Processes and Landforms*, *26*, 1237–1248. https://doi.org/10.1002/esp.261

Browne, G. H., & Naish, T. R. (2003). Facies development and sequence architecture of a late Quaternary fluvial-marine transition, Canterbury Plains and shelf, New Zealand: Implications for forced regressive deposits. *Sedimentary Geology*, *158*(1–2), 57–86. https://doi.org/10.1016/s0037-0738(02)00258-0

Carter, L., Carter, R. M., McCave, I. N., & Gamble, J. (1996). Regional sediment recycling in the abyssal Southwest Pacific Ocean. *Geology*, *24*(8), 735–738. https://doi.org/10.1130/0091-7613(1996)024<0735:rsrita>2.3.co;2

Carter, L., Neil, H. L., & McCave, I. N. (2000). Glacial to interglacial changes in non-carbonate and carbonate accumulation in the SW Pacific Ocean, New Zealand. *Palaeogeography, Palaeoclimatology, Palaeoecology*, *162*, 333–356. https://doi.org/10.1016/s0031-0182(00)00137-1

Carter, L., Neil, H. L., & Northcote, L. (2002). Late Quaternary ice-rafting events in the SW Pacific Ocean, off eastern New Zealand. *Marine Geology*, *191*(1–2), 19–35. https://doi.org/10.1016/s0025-3227(02)00509-1

Carter, L., Nelson, C. S., Neil, H. L., & Froggatt, P. C. (1995). Correlation, dispersal, and preservation of the Kawakawa Tephra and other late Quaternary tephra layers in the Southwest Pacific Ocean. *New Zealand Journal of Geology and Geophysics*, *38*, 29–46. https://doi.org/10.1080/00288306.1995.9514637

Carter, R. M., & Gammon, P. (2004). New Zealand maritime glaciation: Millennial-scale Southern climate change since 3.9 Ma. *Science*, *304*, 1659–1662. https://doi.org/10.1126/science.1093726

Carter, R. M., McCave, I. N., Richter, C., Carter, L., Aita, Y., Buret, C., et al. (1999). Site 1122: Turbidites with a contourite foundation. Proceedings of the Ocean Drilling Programme. Initial Reports, 181. https://doi.org/10.2973/odp.proc.ir.181.106.2000

Costa, K. M., Hayes, C. T., Anderson, R. F., Pavia, F. J., Bausch, A., Deng, F., et al. (2020). ^{230}Th normalization: New insights on an essential tool for quantifying sedimentary fluxes in the modern and Quaternary ocean. *Paleoceonography and Paleoclimatology*, *35*(2). e2019PA003820,. https://doi.org/10.1029/2019pa003820

Dadey, K. A., Janecek, T., & Klaus, A. (1992). Dry-bulk density: Its use and determination. Proceedings of the ocean drilling program, scientific results. National Science Foundation, & Joint Oceanographic Institutions Incorporated.

De Deckker, P., Norman, M., Goodwin, I. D., Wain, A., & Gingele, F. X. (2010). Lead isotopic evidence for an Australian source of aeolian dust to Antarctica at times over the last 170,000years. *Palaeogeography, Palaeoclimatology, Palaeoecology*, *285*(3–4), 205–223. https://doi.org/10.1016/j.palaeo.2009.11.013

Delmonte, B., Basile-Doelsch, I., Petit, J.-R., Maggi, V., Revel-Rolland, M., Michard, A., et al. (2004). Comparing the Epica and Vostok dust records during the last 220,000 years: Stratigraphical correlation and provenance in glacial periods. *Earth-Science Reviews 66*(1–2), 63–87. https://doi.org/10.1016/j.earscirev.2003.10.004

Ding, X., Wu, Y., & Li, W. (2017). 0.9 Ma oxygen isotope stratigraphy for a shallow-water sedimentary transect across three IODP 317 sites in the Canterbury Bight of the southwest Pacific Ocean. *Palaeogeography, Palaeoclimatology, Palaeoecology*, *465*(A), 1–13. https://doi.org/10.1016/j.palaeo.2016.10.008

Dunbar, N. W., Iverson, N. A., Van Eaton, A. R., Sigl, M., Alloway, B. V., Kurbatov, A. V., et al. (2017). New Zealand supereruption provides time marker for the last glacial maximum in Antarctica. *Scientific Reports*, *7*, 12238. https://doi.org/10.1038/s41598-017-11758-0

Dymond, J., Suess, E., & Lyle, M. (1992). Barium in deep-sea sediment: A geochemical proxy for paleoproductivity. *Paleoceanography*, *7*(2), 163–181. https://doi.org/10.1029/92pa00181

Eden, D. N., & Hammond, A. P. (2003). Dust accumulation in the New Zealand region since the last glacial maximum. *Quarternary Science Reviews*, *22*(18–19), 2037–2052. https://doi.org/10.1016/s0277-3791(03)00168-9

Gersonde, R. (Ed.), (2011). *The expedition of the research vessel "Polarstern" to the polar South Pacific in 2009/2010 (ANT-XXVI/2 – BIPOMAC)*. Alfred Wegener Institute for Polar and Marine Research. https://doi.org/10.2312/BzPM_0632_2011

Gibb, J. G., & Adams, J. (1982). A sediment budget for the east coast between Oamaru and Banks Peninsula, South Island, New Zealand. *New Zealand Journal of Geology and Geophysics*, *25*(3), 335–352. https://doi.org/10.1080/00288306.1982.10421497

Ginoux, P., Chin, M., Tegen, I., Prospero, J. M., Holben, B., Dubovik, O., et al. (2001). Sources and distributions of dust aerosols simulated with the GOCART model. *Journal of Geophysical Research*, *106*(D17). 22055–22074. https://doi.org/10.1029/2000jd000053

Grousset, F. E., & Biscaye, P. E. (2005). Tracing dust sources and transport patterns using Sr, Nd and Pb isotopes. *Chemical Geology*, *222*(3–4), 149–167. https://doi.org/10.1016/j.chemgeo.2005.05.006

Grousset, F. E., Biscaye, P. E., Revel, M., Petit, J.-R., Pye, K., Joussaume, S., & Jouzel, J. (1992). Antarctic (Dome C) ice-core dust at 18 k.y. B.P.: Isotopic constraints on origins. *Earth and Planetary Science Letters*, *111*(1), 175–182. https://doi.org/10.1016/0012-821x(92)90177-w

Guo, Z. T., Ruddiman, W. F., Hao, Q. Z., Wu, H. B., Qiao, Y. S., Zhu, R. X., et al. (2002). Onset of Asian desertification by 22 Myr ago inferred from loess deposits in China. *Nature*, *416*, 159–163. https://doi.org/10.1038/416159a

Hall, I. R., McCave, I. N., Shackleton, N. J., Weedon, G. P., & Harris, S. E. (2001). Intensified deep Pacific inflow and ventilation in Pleistocene glacial times. *Nature*, *412*, 809–812. https://doi.org/10.1038/35090552

Hennekam, R., & de Lange, G. (2012). X-ray fluorescence core scanning of wet marine sediments: Methods to improve quality and reproducibility of high-resolution paleoenvironmental records. *Lminology and Oceonography: Methods*, *10*, 991–1003. https://doi.org/10.4319/lom.2012.10.991

Hesse, P. P. (1994). The record of continental dust from Australia in Tasman Sea sediments. *Quarternary Science Reviews*, *13*, 257–272. https://doi.org/10.1016/0277-3791(94)90029-9

Hesse, P. P., & McTainsh, G. H. (1999). Last glacial maximum to early Holocene wind strength in the mid-latitudes of the Southern hemisphere from aeolian dust in the Tasman Sea. *Quaternary Research*, *52*(3), 343–349. https://doi.org/10.1006/qres.1999.2084

Hodell, D., Crowhurst, S., Skinner, L., Tzedakis, P. C., Margari, V., Channell, J. E. T., et al. (2013). Response of Iberian Margin sediments to orbital and suborbital forcing over the past 420 ka. *Paleoceanography*, *28*(1), 185–199. https://doi.org/10.1002/palo.20017

Holt, K. A., Wallace, R. C., Neall, V. E., Kohn, B. P., & Lowe, D. J. (2010). Quaternary tephra marker beds and their potential for palaeoenvironmental reconstruction on Chatham Island, east of New Zealand, southwest Pacific Ocean. *Journal of Quaternary Sciences*, *25*(7), 1169–1178. https://doi.org/10.1002/jqs.1397

Hovan, S. A., Rea, D. K., Pisias, N. G., & Shackleton, N. J. (1989). A direct link between the China loess and marine $\delta^{18}O$ records: Aeolian flux to the north Pacific. *Nature*, *340*, 296–298. https://doi.org/10.1038/340296a0

Jaeschke, A., Wengler, M., Hefter, J., Ronge, T. A., Geibert, W., Mollenhauer, G., et al. (2017). A biomarker perspective on dust, productivity, and sea surface temperature in the Pacific sector of the Southern Ocean. *Geochimica et Cosmochimica Acta*, *204*, 120–139. https://doi.org/10.1016/j.gca.2017.01.045

Jickells, T. D., An, Z. S., Andersen, K. K., Baker, A. R., Bergametti, G., Brooks, N., et al. (2005). Global iron connections between desert dust, ocean biogeochemistry, and climate. *Science*, *308*(5718), 67–71. https://doi.org/10.1126/science.1105959

Joussaume, S. (1993). Paleoclimatic tracers: An investigation using an atmospheric general circulation model under ice age conditions: 1. Desert dust. *Journal of Geophysical Research*, *98*(D2), 2767–2805. https://doi.org/10.1029/92jd01921

Jouzel, J., Masson-Delmotte, V., Cattani, O., Dreyfus, G., Falourd, S., Hoffmann, G., et al. (2007). Orbital and millennial Antarctic climate variability over the past 800,000 years. *Science*, *317*(5839), 793–796. https://doi.org/10.1126/science.1141038

Koffman, B. G., Goldstein, S. L., Winckler, G., Borunda, A., Kaplan, M. R., Bolge, L., et al. (2021). New Zealand as a source of mineral dust to the atmosphere and ocean. *Quarternary Science Reviews*, *251*, 106659. https://doi.org/10.1016/j.quascirev.2020.106659

Kohfeld, K. E., Graham, R. M., De Boer, A. M., Sime, L. C., Wolff, E. W., Le Quéré, C., & Bopp, L. (2013). Southern Hemisphere westerly wind changes during the Last Glacial Maximum: Paleo-data synthesis. *Quarternary Science Reviews*, *68*, 76–95. https://doi.org/10.1016/j.quascirev.2013.01.017

Kohfeld, K. E., & Harrison, S. P. (2001). DIRTMAP: The geological record of dust. *Earth Science-Reviews*, *54*(1–3), 81–114. https://doi.org/10.1016/s0012-8252(01)00042-3

Köhler, P., Bintanja, R., Fischer, H., Joos, F., Knutti, R., Lohmann, G., & Masson-Delmotte, V. (2010). What caused Earth's temperature variations during the last 800,000 years? Data-based evidence on radiative forcing and constraints on climate sensitivity. *Quarternary Science Reviews*, *29*(1–2), 129–145. https://doi.org/10.1016/j.quascirev.2009.09.026

Kohn, B. P., Pillans, B., & McGlone, M. S. (1992). Zircon fission track age for middle Pleistocene Rangitawa Tephra, New Zealand: Stratigraphic and paleoclimatic significance. *Palaeogeography, Palaeoclimatology, Palaeoecology*, *95*, 73–94. https://doi.org/10.1016/0031-0182(92)90166-3

Kotov, S., & Pälike, H. (2018). *QAnalySeries – A cross-platform time series tuning and analysis tool*. American Geophysical Union Fall Meeting Abstracts. Software available at: https://www.marum.de/en/Dr.-sergei-kotov/Software-2.html

Lambert, F., Delmonte, B., Petit, J. R., Bigler, M., Kaufmann, P. R., Hutterli, M. A., et al. (2008). Dust-climate couplings over the past 800,000 years from the EPICA Dome C ice core. *Nature*, *452*, 616–619. https://doi.org/10.1038/nature06763

Lamy, F., Gersonde, R., Winckler, G., Esper, O., Jaeschke, A., Kuhn, G., et al. (2014). Increased dust deposition in the Pacific Southern Ocean during glacial periods. *Science*, *343*(6169), 403–407. https://doi.org/10.1126/science.1245424

Land, M., Wust, R. A., Robert, C., & Carter, R. M. (2010). Plio-Pleistocene paleoclimate in the Southwest Pacific as reflected in clay mineralogy and particle size at ODP Site 1119, SE New Zealand. *Marine Geology*, *274*(1–4), 165–176. https://doi.org/10.1016/j.margeo.2010.04.001

Li, F., Ginoux, P., & Ramaswamy, V. (2008). Distribution, transport, and deposition of mineral dust in the Southern Ocean and Antarctica: Contribution of major sources. *Journal of Geophysical Research*, *113*(D10). https://doi.org/10.1029/2007jd009190

Lisiecki, L. E., & Raymo, M. E. (2005). A Pliocene-Pleistocene stack of 57 globally distributed benthic $\delta^{18}O$ records. *Paleoceanography*, *20*. https://doi.org/10.1029/2004pa001071

Liu, T. S. (Ed.), (1985). *Loess and the environment*. China Ocean Press.

Lohmann, U., & Feichter, J. (2005). Global indirect aerosol effects: A review. *Atmospheric Chemistry and Physics*, *5*, 715–737. https://doi.org/10.5194/acp-5-715-2005

Lourens, L. J., Wehausen, R., & Brumsack, H. J. (2001). Geological constraints on tidal dissipation and dynamical ellipticity of the Earth over the past three million years. *Nature*, *409*, 1029–1033. https://doi.org/10.1038/35059062

Lunt, D. J., & Valdes, P. J. (2002). Dust deposition and provenance at the Last Glacial Maximum and present day.*Geophysical Research Letters*, *29*(22). 42-1–42-4. https://doi.org/10.1029/2002gl015656

Ma, M., Liu, X., Pillans, B. J., Hu, S., Lü, B., & Liu, H. (2013). Magnetic properties of dashing rocks loess at Timaru, South Island, New Zealand. *Geophysical Journal International*, *195*(1), 75–85. https://doi.org/10.1093/gji/ggt206

Maher, B. A., Prospero, J. M., Mackie, D., Gaiero, D., Hesse, P. P., & Balkanski, Y. (2010). Global connections between aeolian dust, climate and ocean biogeochemistry at the present day and at the last glacial maximum. *Earth-Science Reviews*, *99*(1–2), 61–97. https://doi.org/10.1016/j.earscirev.2009.12.001

Mahowald, N. M., Muhs, D. R., Levis, S., Rasch, P. J., Yoshika, M., Zender, C. S., et al. (2006). Changes in atmospheric mineral aerosols in response to climate: Last glacial period, preindustrial, modern, and doubled carbon dioxide climates. *Journal of Geophysical Research*, *111*(D10). https://doi.org/10.1029/2005jd006653

Martin, J. H., Gordon, M., & Fitzwater, S. E. (1991). The case for iron. *Limnology & Oceanography*, *36*(8), 1793–1802. https://doi.org/10.4319/lo.1991.36.8.1793

Martínez-García, A., Rosell-Melé, A., Geibert, W., Gersonde, R., Masqué, P., Gaspari, V., et al. (2009). Links between iron supply, marine productivity, sea surface temperature, and CO_2 over the last 1.1 Ma. *Paleoceanography*, *24*(1). https://doi.org/10.1029/2008pa001657

Martínez-Garcia, A., Rosell-Melé, A., Jaccard, S. L., Geibert, W., Sigman, D. M., & Haug, G. H. (2011). Southern Ocean dust-climate coupling over the past four million years. *Nature*, *476*, 312–315. https://doi.org/10.1038/nature10310

Martínez-García, A., Sigman, D. M., Ren, H., Anderson, R. F., Straub, M., Hodell, D. A., et al. (2014). Iron fertilization of the Subantarctic Ocean during the last ice age. *Science*, *343*(6177), 1347–1350. https://doi.org/10.1126/science.1246848

Marx, S. K., Kamber, B. S., & McGowan, H. A. (2005). Provenance of long-traveled dust determined with ultra-trace-element composition: a pilot study with samples from New Zealand glaciers. *Earth Surface Processes and Landforms*, *30*(6), 699–716. https://doi.org/10.1002/esp.1169

Masson-Delmotte, V., Stenni, B., Pol, K., Braconnot, P., Cattani, O., Falourd, S., et al. (2010). EPICA Dome C record of glacial and interglacial intensities. *Quaternary Science Reviews*, *29*(1–2), 113–128. https://doi.org/10.1016/j.quascirev.2009.09.030

McCave, I. N., & Andrews, J. T. (2019). Distinguishing current effects in sediments delivered to the ocean by ice. I. Principles, methods and examples. *Quaternary Science Reviews*, *212*, 92–107. https://doi.org/10.1016/j.quascirev.2019.03.031

McCave, I. N., Carter, L., & Hall, I. R. (2008). Glacial-interglacial changes in water mass structure and flow in the SW Pacific Ocean. *Quaternary Science Reviews*, *27*(19–20), 1886–1908. https://doi.org/10.1016/j.quascirev.2008.07.010

McCave, I. N., & Hall, I. R. (2006). Size sorting in marine muds: Processes, pitfalls, and prospects for paleoflow-speed proxies. *Geochemistry, Geophysics, Geosystems*, *7*(10). https://doi.org/10.1029/2006gc001284

McCave, I. N., Manighetti, B., & Robinson, S. G. (1995). Sortable silt and fine sediment size/composition slicing: Parameters for palaeocurrent speed and paleoceanography. *Paleoceanography*, *10*(3), 593–610. https://doi.org/10.1029/94pa03039

McCave, I. N., Thornalley, D. J. R., & Hall, I. R. (2017). Relation of sortable silt grain-size to deep-sea current speeds: Calibration of the 'Mud Current Meter'. *Deep Sea Research I: Oceanographic Research Papers*, *127*, 1–12. https://doi.org/10.1016/j.dsr.2017.07.003

McCave, N. (2020). Direct measures of the vigor of ocean circulation via particle grain size. *Oceanography*, *33–2*, 53–55

McConnell, J. R., Aristarain, A. J., Banta, J. R., Edwards, P. R., & Simoes, J. C. (2007). 20th-Century doubling in dust archived in an Antarctic Peninsula ice core parallels climate change and desertification in South America. *Proceedings of the National Academy of Sciences*, *104*(14), 5743–5748. https://doi.org/10.1073/pnas.0607657104

McCraw, J. D. (1975). Quaternary Airfall Deposits of New Zealand. Royal Society of New Zealand Bulletin.

McGlone, M. S., Turney, C. S. M., Wilmshurst, J. M., Renwick, J., & Pahnke, K. (2010). Divergent trends in land and ocean temperature in the Southern Ocean over the past 18,000 years. *Nature Geoscience*, *3*(9), 622–626. https://doi.org/10.1038/ngeo931

Moore, C. M., Mills, M. M., Arrigo, K. R., Berman-Frank, I., Bopp, L., Boyd, P. W., et al. (2013). Processes and patterns of oceanic nutrient limitation. *Nature Geoscience*, *6*, 701–710. https://doi.org/10.1038/ngeo1765

Neff, P. D., & Bertler, N. A. N. (2015). Trajectory modeling of modern dust transport to the Southern Ocean and Antarctica. *Journal of Geophysical Research: Atmospheres*, *120*, 9303–9322. https://doi.org/10.1002/2015jd023304

Nelson, C. S., Hendy, C. H., Jarrett, G. R., & Cuthbertson, A. M. (1985). Near-synchroneity of New Zealand alpine glaciations and Northern Hemisphere continental glaciations during the past 750 kyr. *Nature*, *318*, 361–363. https://doi.org/10.1038/318361a0

Pahnke, K., Zahn, R., Elderfield, H., & Schulz, M. (2003). 340,000-year centennial-scale marine record of southern hemisphere climatic oscillation. *Science*, *301*(5635), 948–952. https://doi.org/10.1126/science.1084451

Paillard, D., Labeyrie, L., & Yiou, P. (1996). Macintosh program performs time-series analysis. *Eos Transactions AGU*, *77*(39), 379. https://doi.org/10.1029/96eo00259

Paterson, G. A., & Heslop, D. (2015). New methods for unmixing sediment grain size data. *Geochemistry, Geophysics, Geosystems*, *16*(12), 4494–4506. https://doi.org/10.1002/2015gc006070

Peterson, L. C., Haug, G. H., Hughen, K. A., & Röhl, U. (2000). Rapid changes in the hydrologic cycle of the Tropical Atlantic during the last glacial. *Science*, *290*(5498), 1947–1951. https://doi.org/10.1126/science.290.5498.1947

Petit, J. R., Mourner, L., Jouzel, J., Korotkevich, Y. S., Kotlyakov, V. I., & Lorius, C. (1990). Paleoclimatological and chronological implications of the Vostok core dust record. *Nature*, *343*, 56–58. https://doi.org/10.1038/343056a0

Pillans, B. (2003). Subdividing the Pleistocene using the Matuyama-Brunhes boundary (MBB): An Australasian perspective. *Quaternary Science Reviews*, *22*, 1569–1577. https://doi.org/10.1016/s0277-3791(03)00078-7

Pillans, B., Kohn, B. P., Berger, G., Froggatt, P., Duller, G., Alloway, B., & Hesse, P. (1996). Multi-method dating comparison for Mid-Pleistocene Rangitawa Tephra, New Zealand. *Quaternary Science Reviews*, *15*, 641–653. https://doi.org/10.1016/0277-3791(96)00035-2

Pillans, B., McGlone, M., Palmer, A., Mildenhall, D., Alloway, B., & Berger, G. (1993). The last glacial maximum in central and southern North Island, New Zealand: A paleoenvironmental reconstruction using the Kawakawa Tephra Formation as a chronostratigraphic marker. *Palaeogeography, Palaeoclimatology, Palaeoecology*, *101*, 283–304. https://doi.org/10.1016/0031-0182(93)90020-j

Prospero, J. M., Ginoux, P., Torres, O., Nicholson, S. E., & Gill, T. E. (2002). Environmental characterization of global sources of atmospheric soil dust identified with the NIMBUS 7 Total Ozone Mapping Spectrometer (TOMS) absorbing aerosol product. *Reviews of Geophysics*, *40*(1), 1002. https://doi.org/10.1029/2000rg000095

Putnam, A. E., Denton, G. H., Schaefer, J. M., Barrell, D. J. A., Andersen, B. G., Finkel, R. C., et al. (2010). Glacier advance in southern middle-latitudes during the Antarctic Cold Reversal. *Nature Geosciences*, *3*(10), 700–704. https://doi.org/10.1038/ngeo962

Putnam, A. E., Schaefer, J. M., Denton, G. H., Barrell, D. J. A., Birkel, S. D., Andersen, B. G., et al. (2013). The last glacial maximum at 44°S documented by a 10Be moraine chronology at Lake Ohau, Southern Alps of New Zealand. *Quaternary Science Reviews*, *62*, 114–141. https://doi.org/10.1016/j.quascirev.2012.10.034

Qi, L., Hu, J., & Gregoire, D. C. (2000). Determination of trace elements in granites by inductively coupled plasma mass spectrometry. *Talanta*, *51*(3), 507–513

Raeside, J. D. (1964). Loess deposits of the South Island, New Zealand, and soils formed on them. *New Zealand Journal of Geology and Geophysics*, *7*(4), 811–838. https://doi.org/10.1080/00288306.1964.10428132

Rea, D. K. (1994). The paleoclimatic record provided by eolian deposition in the deep sea: The geologic history of wind. *Reviews of Geophysics*, *32*(2), 159–195. https://doi.org/10.1029/93rg03257

Rea, D. K., Leinen, M., & Janecek, T. R. (1985). Geologic approach to the long-term history of atmospheric circulation. *Science*, *227*(4688), 721–725. https://doi.org/10.1126/science.227.4688.721

Rea, D. K., Snoeckx, H., & Joseph, L. H. (1998). Late Cenozoic eolian deposition in the north Pacific: Asian drying, Tibetan uplift, and cooling of the northern hemisphere. *Paleoceanography*, *13*(3), 215–224. https://doi.org/10.1029/98pa00123

Rees, C., Palmer, A., & Palmer, J. (2019). Quaternary sedimentology and tephrostratigraphy of the lower Pohangina Valley, New Zealand. *New Zealand Journal of Geology and Geophysics*, *62*, 171–194. https://doi.org/10.1080/00288306.2018.1547321

Revelrolland, M., Dedeckker, P., Delmonte, B., Hesse, P., Magee, J., Basiledoelsch, I., et al. (2006). Eastern Australia: A possible source of dust in East Antarctica interglacial ice. *Earth and Planetary Letters*, *249*(1–2), 1–13. https://doi.org/10.1016/j.epsl.2006.06.028

Rohling, E. J., Sluijs, A., Dijkstra, H. A., Köhler, P., van de Wal, R. S. W., von der Heydt, A. S., et al. (2012). Making sense of palaeoclimate sensitivity. *Nature*, *491*, 683–691

Ronge, T. A., Tiedemann, R., Lamy, F., Köhler, P., Alloway, B. V., De Pol-Holz, R., et al. (2016). Radiocarbon constraints on the extent and evolution of the South Pacific glacial carbon pool. *Nature Communications*, *7*, 11487. https://doi.org/10.1038/ncomms11487

Russell, J. L., Dixon, K. W., Gnanadesikan, A., Stouffer, R. J., & Toggweiler, J. R. (2006). The Southern Hemisphere westerlies in a warming world: Propping open the door to the deep ocean. *Journal of Climate*, *19*(24), 6382–6390. https://doi.org/10.1175/jcli3984.1

Shao, Y., Wyrwoll, K.-H., Chappell, A., Huang, J., Lin, Z., McTainsh, G. H., et al. (2011). Dust cycle: An emerging core theme in Earth system science. *Aeolian Research*, *2*(4), 181–204. https://doi.org/10.1016/j.aeolia.2011.02.001

Shoenfelt, E. M., Winckler, G., Annett, A. L., Hendry, K. R., & Bostick, B. C. (2019). Physical weathering intensity controls bioavailable primary iron(II) silicate content in major global dust sources. *Geophysical Research Letters*, *46*(19), 10854–10864. https://doi.org/10.1029/2019gl084180

Shoenfelt, E. M., Winckler, G., Lamy, F., Anderson, R. F., & Bostick, B. C. (2018). Highly bioavailable dust-borne iron delivered to the Southern Ocean during glacial periods. *Proceedings of the National Academy of Sciences of the United States of America*, *115*(44), 11180–11185. https://doi.org/10.1073/pnas.1809755115

Shulmeister, J., Goodwin, I., Renwick, J., Harle, K., Armand, L., McGlone, M. S., et al. (2004). The Southern Hemisphere westerlies in the Australasian sector over the last glacial cycle: A synthesis. *Quaternary International*, *118–119*, 23–53. https://doi.org/10.1016/s1040-6182(03)00129-0

Shulmeister, J., Thackray, G. D., Rittenour, T. M., Fink, D., & Patton, N. R. (2019). The timing and nature of the last glacial cycle in New Zealand. *Quaternary Science Reviews*, *206*, 1–20. https://doi.org/10.1016/j.quascirev.2018.12.020

Sime, L. C., Kohfeld, K. E., Le Quéré, C., Wolff, E. W., de Boer, A. M., Graham, R. M., & Bopp, L. (2013). Southern Hemisphere westerly wind changes during the Last Glacial Maximum: Model-data comparison. *Quaternary Science Reviews*, *64*, 104–120. https://doi.org/10.1016/j.quascirev.2012.12.008

Spratt, R. M., & Lisiecki, L. E. (2016). A Late Pleistocene sea level stack. *Climate of the Past*, *12*(4), 1079–1092. https://doi.org/10.5194/cp-12-1079-2016

Stewart, R. B., & Neall, V. E. (1984). Chronology of paleoclimatic change at the end of the last glaciation. *Nature*, *311*, 47–48. https://doi.org/10.1038/311047a0

Struve, T., Pahnke, K., Lamy, F., Wengler, M., Böning, P., & Winckler, G. (2020). A circumpolar dust conveyor in the glacial Southern Ocean. *Nature Communications*, *11*(1), 1–11. https://doi.org/10.1038/s41467-020-18858-y

Tagliabue, A., Bowie, A. R., Boyd, P. W., Buck, K. N., Johnson, K. S., & Saito, M. A. (2017). The integral role of iron in ocean biogeochemistry. *Nature*, *543*, 51–59. https://doi.org/10.1038/nature21058

Taylor, S. R., & McLennan, S. M. (1995). The geochemical evolution of the continental crust. *Reviews of Geophysics*, *33*, 241–265. https://doi.org/10.1029/95rg00262

Thiede, J. (1979). Wind regimes over the late Quaternary southwest Pacific Ocean. *Geology*, *7*(5), 259–262. https://doi.org/10.1130/0091-7613(1979)7<259:wrotlq>2.0.co;2

Thiede, J., Nees, S., Schulz, H., & De Deckker, P. (1997). Oceanic surface conditions recorded on the sea floor of the Southwest Pacific Ocean through the distribution of foraminifers and biogenic silica. *Paleogeography, Palaeoclimatology, Palaeoecology*, *131*(3–4), 207–239. https://doi.org/10.1016/s0031-0182(97)00004-7

Thomson, J., Croudace, I. W., & Rothwell, R. G. (2006). *A geochemical application of the ITRAX scanner to a sediment core containing eastern Mediterranean sapropel units*. In R. G. Rothwell, (Ed.), New techniques in sediment core analysis (*267*, pp. 65–77). Geological Society of London Special Publication. https://doi.org/10.1144/GSL.SP.2006.267.01.05

Tournadre, J., Bouhier, N., Girard-Ardhuin, F., & Rémy, F. (2016). Antarctic icebergs distributions 1992-2014. *Journal of Geophysical Research: Oceans*, *121*(1), 327–349. https://doi.org/10.1002/2015jc011178

Trudgill, M. D., Shuttleworth, R., Bostock, H. C., Burke, A., Cooper, M. J., Greenop, R., & Foster, G. L. (2020). The flux and provenance of dust delivered to the SW Pacific during the Last Glacial Maximum. *Paleoceanography and Paleoclimatology*, *35*. e2020PA003869. https://doi.org/10.1029/2020pa003869

Turekian, K. K., & Wedepohl, K. H. (1961). Distribution of the elements in some major units of the earth's crust. *Geological Society of American Bulletin*, *72*(2), 175–192. https://doi.org/10.1130/0016-7606(1961)72[175:doteis]2.0.co;2

Vallelonga, P., van de Velde, K., Candelone, J.-P., Morgan, V. I., Boutron, C. F., & Rosman, K. J. R. (2002). The lead pollution history of Law Dome, Antarctica, from isotopic measurements on ice cores: 1500 AD to 1989 AD. *Earth and Planetary Sciences Letters*, *204*(1–2), 291–306. https://doi.org/10.1016/s0012-821x(02)00983-4

Vandergoes, M. J., Hogg, A. G., Lowe, D. J., Newnham, R. M., Denton, G. H., Southon, J., et al. (2013). A revised age for the Kawakawa/Oruanui tephra, a key marker for the last glacial maximum in New Zealand. *Quarternary Science Reviews*, *74*, 195–201. https://doi.org/10.1016/j.quascirev.2012.11.006

Veres, D., Bazin, L., Landais, A., Toyé Mahamadou Kele, H., Lemieux-Dudon, B., Parrenin, F., et al. (2013). The Antarctic ice core chronology (AICC2012): An optimized multi-parameter and multi-site dating approach for the last 120 thousand years. *Climate of the Past*, *9*, 1733–1748. https://doi.org/10.5194/cp-9-1733-2013

Wagener, T., Guieu, C., Losno, R., Bonnet, S., & Mahowald, N. (2008). Revisiting atmospheric dust export to the Southern Hemisphere ocean: Biogeochemical implications. *Global Biochemical Cycles*, *22*(2). https://doi.org/10.1029/2007gb002984

Walter, H. J., Hegner, E., Diekmann, B., Kuhn, G., & Rutgers van der loeff, M. M. (2000). Provenance and transport of terrigenous sediment in the South Atlantic Ocean and their relations to glacial and interglacial cycles: Nd and Sr isotopic evidence. *Geochimica et Cosmochimica Acta*, *64*(22), 3813–3827. https://doi.org/10.1016/s0016-7037(00)00476-2

Weeks, R., Laj, C., Endignoux, L., Fuller, M., Roberts, A., Manganne, R., et al. (1993). Improvements in long-core measurement techniques: applications in palaeomagnetism and paleoceanography. *Geophysical Journal International*, *114*, 651–662. https://doi.org/10.1111/j.1365-246x.1993.tb06994.x

Weltje, G. J., Bloemsma, M. R., Tjallingii, R., Heslop, D., Röhl, U., & Croudace, I. W. (2015). Prediction of geochemical composition from XRF core scanner data: A new multivariate approach including automatic selection of calibration samples and quantification of uncertainties. In *Micro-XRF studies of sediment cores* (pp. 507–534). Springer. http://dx.doi.org/10.1007/978-94-017-9849-5-21

Wengler, M., Lamy, F., Struve, T., Borunda, A., Böning, P., Geibert, W., et al. (2019). A geochemical approach to reconstruct modern dust fluxes and sources to the South Pacific. *Geochimica et Cosmochimica Acta*, *264*, 205–223. https://doi.org/10.1016/j.gca.2019.08.024

Ziegler, M., Jilbert, T., de Lange, G. J., Lourens, L. J., & Reichart, G.-J. (2008). Bromine counts from XRF scanning as an estimate of the marine organic carbon content of sediment cores. *Geochemistry, Geophysics, Geosystems*, *9*(5). https://doi.org/10.1029/2007gc001932